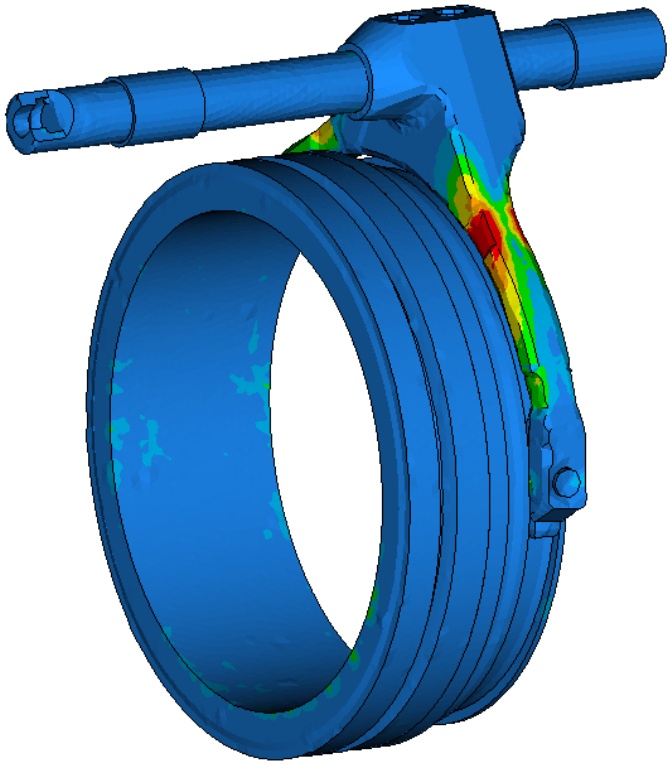

# From Data to Simulation: A dynamic shift fork analysis

## A correlation study between dynamic explicit FEA and empirical test data on shift forks

Master thesis at Mechanics and Maritime Science, M2

ELIN FAHLGREN
EDVIN ÅKESON

**Department of Mechanics and Maritime Sciences**

CHALMERS UNIVERSITY OF TECHNOLOGY
Gothenburg, Sweden 2024
www.chalmers.se

MASTER'S THESIS 2024:02

# From Data to Simulation: A dynamic shift fork analysis

A correlation study between dynamic explicit FEA and empirical test data on shift fork

ELIN FAHLGREN
EDVIN ÅKESON


CHALMERS
UNIVERSITY OF TECHNOLOGY

Department of Mechanics and Maritime Sciences
*Division of Dynamics*
Chalmers University of Technology
Gothenburg, Sweden 2024

From Data to Simulation: A dynamic shift fork analysis
A correlation study between dynamic explicit FEA and empirical test data on shift fork
ELIN FAHLGREN
EDVIN ÅKESON



Supervisor: Axel Josefsson, Volvo Group Trucks Technology
Examiner: Jim Brouzoulis, Chalmers Department of Mechanics and Maritime Sciences

Master's Thesis 2024:02
Department of Mechanics and Maritime Sciences
Division of Dynamics
Chalmers University of Technology
SE-412 96 Gothenburg
Sweden
Telephone. +46 (0)31 772 1000

Cover: Stress distribution in parts of the transmission range section from META post processor.

Typeset in: LaTeX
Printed by Chalmers Reproservice
Gothenburg, Sweden 2024

# Sammandrag

I en lastbils automat-manuella växellåda sker kopplingar genom att en växlingshylsa förflyttas och ändrar den ingående vridningens bana. Kopplingshylsa förflyttas när en pneumatisk cylinder expanderar eller komprimerar, vilket förflyttar delarna som ingår i 'range'-sektionen i växellådan. De ingående delarna är en skiftstång, en kuggring och en växelgaffel. Målet med denna uppsats är att skapa en modell av detta växlingsförlopp. En explicit dynamisk modell används för att fånga de snabba dynamiska rörelserna och lasterna i systemet. Även en regression skapas för att kunna förutspå vilka töjningar växelgaffeln utsätts för under en tandträff.

Projektet har behandlat testdata från 30 olika växlingar. Randvillkor, initialvillkor och krafter i FE modellen estimeras från dessa. FEA användes för att identifiera parametrar som är viktigast för att beskriva ett växlingsförlopp. Dessa var hastigheten och kraften vid väggträff. Den skapade modellen har ett medelfel för första förskjutningstoppen på 20%, och ett medelfel på 32% för den andra jämfört med testdata. För regressionen är de viktigaste parametrarna acceleration för kuggringen, hastigheten för skiftstången och positionen för kuggringen vid tandträff. Regressionen förklarar 55% av variationen i den uppmätta töjningen.

Sammanfattningsvis innehåller detta projekt flera osäkerheter på grund av att varje växlings fall är unikt. Trots detta stämmer modellresultaten väl överens med data. För att förbättra modellen krävs en djupare undersökning kring dämpningen i systemet.

Nyckelord: FEA, FEM, Explicit, ANSA, ABAQUS, Växellåda, Regression, Emperisk data

# Abstract

In a truck's AMT, gear shifting is performed by moving a sleeve with dog-clutch teeth, to change the load path through the transmission. A pneumatic cylinder pushes the system, which includes a rod, ring gear, and shift fork. Due to the fast transient dynamics, rapid shift and high dynamic loads of the system, an explicit dynamic FE model is used to simulate its behaviour. The aim is to build an FE model of the fork and validate it against empirical test data, as well as find the key parameters to describe the loads from a shift. Additionally, a regression was developed to predict the strain in the fork during tooth collisions.

Boundary conditions, initial conditions, and forces included in the FE model were estimated from empirical data from 30 shifts. FEA was used to identify key parameters affecting the shift. The key parameters found were velocity and net force at impact. The finished model has a 20% average error for the first displacement peak, and a 32% average error for the second, compared to the empirical data. For the regression, the key parameters were the acceleration of the ring gear, the velocity of the rod, and the ring gear position at collision. The regression explains 55% of the strain variation.

In conclusion, the project contains uncertainties due to the uniqueness of every shift. However, the FE results correspond well with the test data but future research into what damping should be used could enhance model accuracy.



Keywords: FEA, FEM, Explicit, ANSA, ABAQUS, Transmission, Regression, Empirical data

# Acknowledgements

We would like to extend our sincere appreciation to VOLVO Group Technologies for providing the resources and environment necessary to carry out this project. The access to data and tools, as well as the collaboration with the skilled professionals at VOLVO GTT, has greatly enriched our learning experience and the overall success of this project.

Furthermore, we would like to express our deepest gratitude to our supervisor, Axel Josefsson, for their invaluable guidance, support, and encouragement throughout this Master's thesis. Their expertise and insights have been instrumental in shaping the direction and quality of our work.

Elin Fahlgren and Edvin Åkeson
Gothenburg, June, 2024

# List with Acronyms

Below is the list of acronyms that have been used throughout this thesis listed in alphabetical order

| | |
|---|---|
| AMT | Automated Manual Transmission |
| CAD | Computer Aided Design |
| DOF | Degree of freedom |
| FE | Finite Element |
| FEA | Finite Element Analysis |
| PID | Property ID in ANSA |
| Volvo GTT | Volvo Group Trucks Technology |

# Table of Content

# List of Figures

# List of Tables

# 1
# Introduction

Since the introduction of finite element simulations, products have been able to be tested virtually instead of physically [1]. This does not completely remove the need for physical testing, but it has allowed for decreased cost of development. This in turn allows for more iterations and concepts to be developed which finally results in a more optimized product and is beneficial for all parties.

One area where these simulations have played a large role is the vehicle industry. It is now commonplace for most new parts of a vehicle to be tested in some way through finite element simulations [2]. The parts and products can for example be tested for mechanical loads, fatigue damage, fluid flow or vibrations, which all play vital roles when the products are in use.

At Volvo trucks, mostly static finite element simulations have been conducted regarding the mechanical loads and displacements when evaluating the shift system of the transmission range section. This thesis will instead conduct simulations in this area using dynamic explicit simulations.

## 1.1 Background

In trucks equipped with an Automated Manual Transmission (AMT), gear shifts are executed through the manipulation of a sleeve, housing dog clutch teeth. The sleeve is actuated by a pneumatic cylinder, which in turn propels a rod attached to a shift fork. Given the imperative need for swift gear changes, the components involved endure substantial dynamic forces.

The magnitude of these forces depends on various factors, including the pressure within the cylinder, the mass and stiffness of the system and the relative velocities of the rotating elements. Adding complexity, the load characteristics fluctuate according to the angle at which the dog clutch teeth engage, resulting in many potential outcomes, where the ring gear can have vastly different velocities and different movements from a small change in input parameters. Some of these input parameters are the differential rotational speed of the ring gear, the angular position at which the connection is attempted and the axial velocity at which the connection is attempted.

To simulate the dynamic behaviour of these shifting components accurately, a FE analysis becomes necessary. Figure 1.1 displays the main parts used to simulate the

dynamic behaviour, the different parts are further explained in Section 2.1. Furthermore, to fine-tune and validate the model, it is essential to establish a correlation with actual testing.

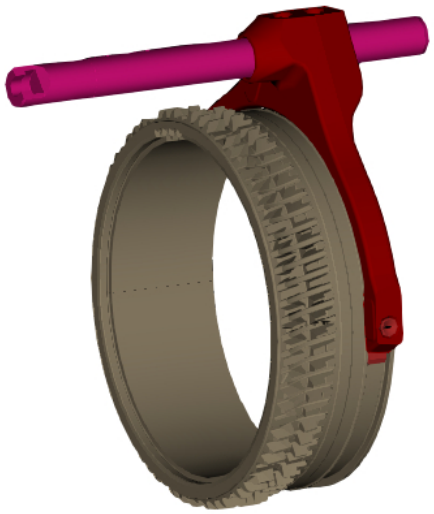

**Figure 1.1:** Main parts of the system used to simulate the dynamic behaviour.

## 1.2 Aim

The project aims to perform explicit dynamic simulations of the shift fork in the AMT's Range section in a Volvo branded truck, to identify key parameters to correlate the simulation with empirical test data. Moreover, a multivariate regression will be created to predict the strain the fork is subjected to when the ring gear and housing clash in both the teeth and end-stop collision.

## 1.3 Objective

The objective of this master's thesis is to develop an explicit Finite Element (FE) simulation model, adapted for ABAQUS, aimed at capturing the dynamic behaviour of a shift fork during gear shifts and subsequently correlating the simulation results with empirical test data, which includes measurements of displacements and forces obtained during physical testing. Furthermore, a regression is created to predict the strain in the fork when the teeth collide during the gear change, this is also created for an end-stop collision. This project will later serve as a foundation for compiling a comprehensive load spectrum representing various types of gear shifts encountered over the lifespan of a transmission. Included in the project objective are the following points:

1. Analyse and compile test data
2. Build a dynamic explicit FE model
3. Identify key parameters for different gear shifts
4. Verify FE model using empirical test data
5. Build a regression predicting the strain for when the teeth collide
6. Build a regression predicting the strain for collision with the end-stop

## 1.4 Limitations

When constructing the model, linear material properties will be used given that most of the components are constructed of steel or forged steel, and the stresses will not surpass the yield limit.

The geometry of the dog teeth will not be meshed and simulated. This would add complexity and increase computational cost. Instead, the sleeves surfaces will be modeled as smooth cylinders. This is a result of the shift fork being the main subject of this analysis, and the force and stress on the sleeve and dog teeth are not of interest. Further, since the FE analysis only will be used when the ring gear shifts against the end-wall, it is assumed that no contact is made by the teeth.

The pneumatic part of the system that actuates the rod attached to the shift fork will be simplified where the movement instead will come from an applied velocity and a spring together with a force which combined equals the velocity and net force that would be produced from the pressure in the pneumatic cylinder.

The project is mostly focused on finding a way to do these types of simulations and investigate their viability so they can be used in the future. Therefore, simulations in this project will be performed using a coarser mesh than would likely be required to get results that can be used to correctly evaluate the risk of failure of the product. A coarser mesh will allow for shortened simulation time, which is of importance given that many different scenarios need to be simulated.

There is a small spring loaded ball on the rod surface that stops the rod from moving and accidentally shifting gears when no input is given, this is called a detent. The geometry and forces of this spring loaded ball will be neglected in the simulation given that they are comparatively small.

The project is limited to VOLVO's AMT main section with a synchronised range section.

The test data used in this project has already been collected, and it is therefore outside the scope of this project to perform more tests.

This project will only be focused on the specific shift when moving from high range to low range. This shift is chosen because it is less complex than shifting from low range to high range and is more suitable for creating a first model. It also reduces the number of shifts that need to be analysed in the limited time frame of the project.

# 2
# Theory

The following chapter explains the used theory to give a deeper understanding of the different parts of the project. This includes information about the transmission range section and information needed to properly construct a simulation model of the system as well as the regression.

## 2.1 Transmission range section

A traditional truck transmission consists of many different parts. The three key sections responsible for the different gears that can be used are the splitter, which can be set to high- or low split, the main section, which contains the main gears, and the range section, which can be set to high- or low range. The different sections can be seen in a 2D sketch in Figure 2.1. Essentially, the main section is responsible for the main gear, the same way a normal cars transmission works. The splitter and range gear are auxiliary sections used to increase or decrease the gear ratio between the input and output shaft. This allows for the 3 main gears to be transformed into 12 different driving gears, depending on what path is taken through the transmission. This project only considers the range section.

The shifting components of the range section consist of a rod that slides through bearings connected to the transmission housing. On the rod, a shift fork is fixed. This shift fork connects to a ring gear, through pads, of a planetary gear set, which houses planet gears as well as sun gear. The ring gear doubles as an engaging sleeve. The range section can be seen on the right side of Figure 2.1. The green central part is the sun gear, the blue surrounding it is the planet gears, and the grey on the outside of the planet gears is the ring gear. The rod is not shown in this image. The ring gear, push rod, shift fork, pads, and housing parts can be seen in Figure 2.2, here the sun and planet gears are removed as well as the gear teeth on the ring gear.

When shifting to low range, the ring gear attaches to teeth in the transmission housing, making it fixed. The sun gear is the input and the carrier is the output. Due to the planet gears and sun gear ratio, the output rotational speed is reduced from the input. When shifting to high range, the ring gear connects to the main shaft, making all 3 parts rotating in unison, and the same input velocity will be transferred to the output shaft. The shift to low or high range is visualized by the two arrows in the top right of Figure 2.1, where HR is high range and LR is low range.

During a shift, the gear exchange is divided into different stages. Initially, the shift is engaged, followed by synchronization before a significant drop. In the middle of the slope, a tooth collision occurs between the teeth and the housing. In the valley, after the drop, the end-stop collision occurs before the shift is engaged again and the process is complete. The process is displayed in Figure 2.3. This project has focused on the tooth and end-wall collisions.

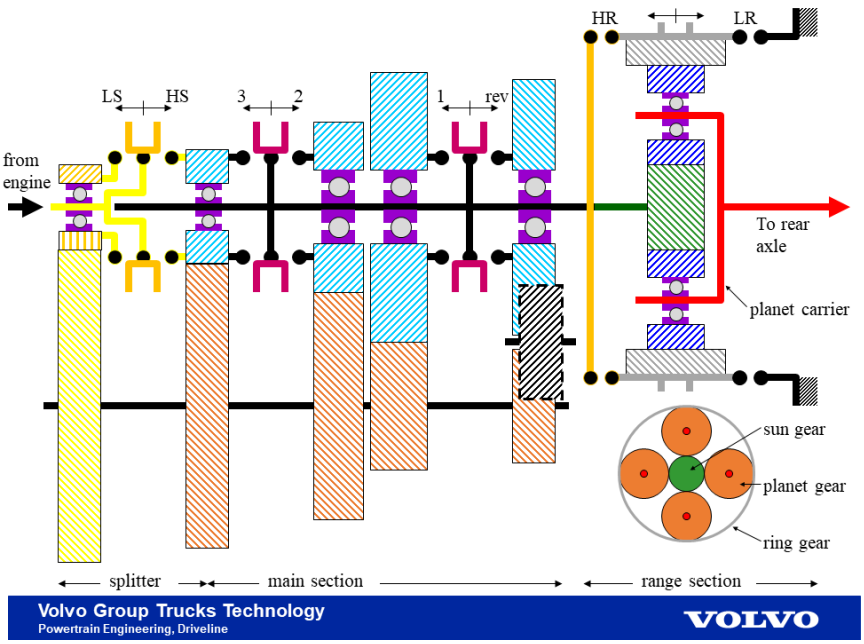


**Figure 2.1:** 2D sketch of the transmission. Adapted from Anders Hedman, Volvo GTT.

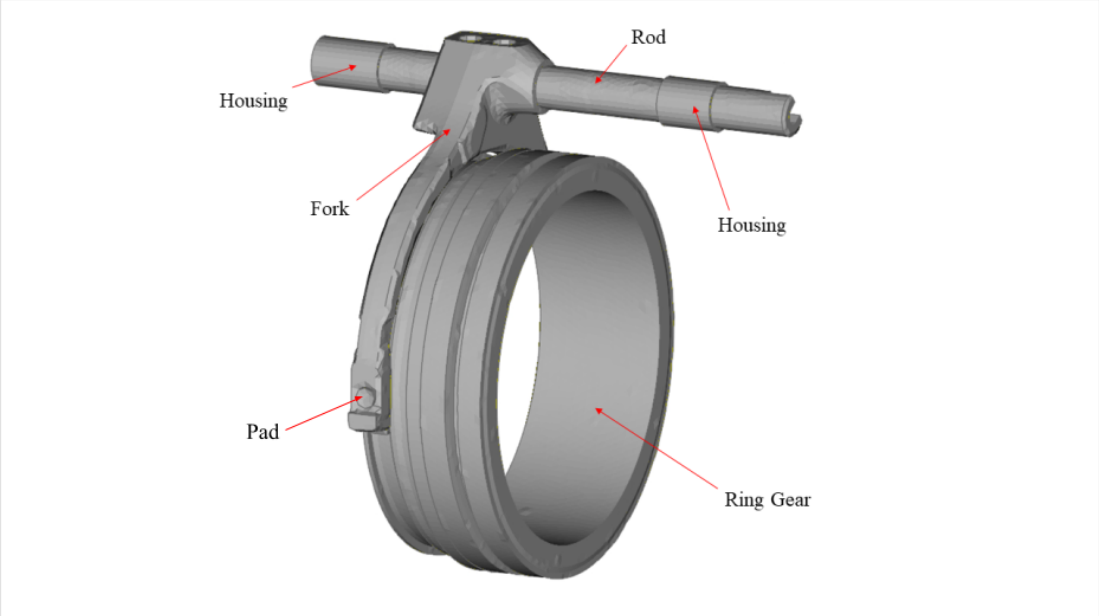


**Figure 2.2:** Simplified 3D model of parts of the range section.

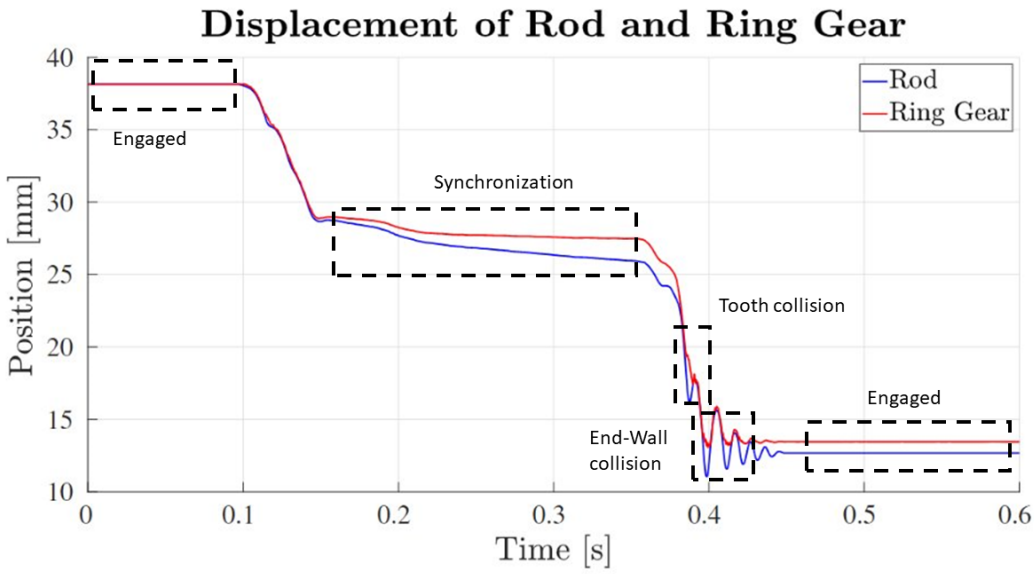


**Figure 2.3:** A typical shift displaying the different stages of the shift process.

## 2.2 Finite element simulation

When choosing simulation type for a problem, a few aspects are to be considered. A static simulation may be used for problems where time dependence and inertia can be neglected. This is suitable when the part of interest has a clear, static loading condition.

A dynamic simulation can be used when time dependant effects are important and when the progression of the system is fast. Dynamic simulations are necessary in for example crash simulations, where the dynamic aspects between all parts of the system affect each other. In this project, an explicit dynamic simulation will be used. An explicit dynamic simulation uses explicit integration in time of the equations of motion which emphasises the importance of speed in the simulation [3]. Dynamic simulations account for changeable conditions during the simulation.

For physical phenomena that require non-linear, transient simulations and fast system progression, an explicit simulation is preferred [3]. Another method for handling time dependent problems is implicit simulations. One advantage with an implicit method, is that it allows for large time increments [4], while explicit has a maximum time step depending on the mesh.

### 2.2.1 Contact

When using an FE simulation, contacts between parts or surfaces are often present. When defining these contacts, different parameters and models are included to ensure that the contact behaves properly and that the solution converges.

#### 2.2.1.1 Contact definitions

There are two general types of contact definitions used in ABAQUS, tie contacts and contact pairs. Tie contacts define that two contact surfaces are fixed together, while a contact pair only defines two surfaces that may come in contact. Both of these definitions require that so-called master and slave surfaces be defined.

#### 2.2.1.2 Master and slave surface

Defining a contact requires two surfaces, a master surface, and a slave surface. These define the area where the contact between two geometries may occur. There are a few criteria to determine which surface should be selected as the slave and master. Generally, the most stiff or strong surface should be defined as the master surface, while the surface with the finest mesh should be defined as the slave [5]. This comes from that the master surface will be allowed to penetrate the slave surface, but not the nodes. Thus, if the slave surface is densely meshed, the slave nodes will efficiently stop the penetration from the master surface. Further, since the stiffest surface is the master, excessive penetration will be prohibited by the more densely meshed slave surface even as it deforms.

#### 2.2.1.3 Contact damping

Contact damping in ABAQUS is a damping mechanism that acts to resist relative motion between surfaces in contact. It can influence the motion normal and the motion tangential to the surfaces which is in interaction [6]. The damping coefficient, in ABAQUS/Explicit, is a proportionality constant expressed in units of pressure divided by velocity [7]. The coefficient remains fixed at the specified constant while the surfaces are interacting, otherwise, the coefficient is zero. Contact damping helps to stabilize and control contact interactions by mitigating some instabilities and oscillations in the contact.

### 2.2.2 Structural damping

In ABAQUS, a general material damping can be introduced in the form of Rayleigh damping. Rayleigh damping is a type of proportional damping used in structural dynamics and dynamic FEA simulations [8]. The dynamic behaviour of a structure is described by Equation (2.1). The equation balances the effects of inertia, stiffness, damping, and external forces, and it is used to analyse the response of structures to dynamic loading conditions and predict their dynamic behaviour over time [9].

$$\mathbf{M}\ddot{\mathbf{u}} + \mathbf{V}\dot{\mathbf{u}} + \mathbf{K}\mathbf{u} = \mathbf{f}(t) \tag{2.1}$$

Rayleigh damping assumes that the damping in the system is distributed as a combination of mass and stiffness. This damping exhibits linear proportionality to the mass and the stiffness of the system. The equation for Rayleigh damping can be seen in Equation (2.2).

$$\xi_i = \frac{\alpha_R}{2\omega_i} + \frac{\beta_R \omega_i}{2} \tag{2.2}$$

$\xi_i$ is the fraction of critical damping while $\alpha_R$ and $\beta_R$ are Rayleigh damping factors. $\omega_i$ is the natural frequency from the mode of interest. Generally, $\alpha_R$ damps the lower frequencies while $\beta_R$ damps the higher frequencies [10]. So for a chosen fraction of critical damping, either $\alpha_R$ or $\beta_R$ can easily be calculated given that the other is assumed to be 0.

### 2.2.3 Mesh

When using a dynamic explicit solver, the mesh element size is a crucial input. The time step needed for convergence is dictated by the smallest element in the mesh according to Equation (2.3), see [11] for details

$$\Delta t = \frac{L^e}{c_d}, \quad c_d = \sqrt{\frac{E}{\rho}} \tag{2.3}$$

where $L^e$ denotes the characteristic length of the smallest element in the mesh, and $c_d$ is the wave speed in the material. This means that it is favourable to not have

a small number of elements of small size since it will affect the solver time for the entire system, and the mesh should be kept as homogeneous as possible. However, if needed, the mesh can be refined in some areas to produce results of higher resolution at the cost of computational resources.

The reason that the time step is important comes from the interaction between the characteristic element length and wave speed. It is possible for the solver to skip an element if the wave speed is such that it can not be captured within the chosen time step. This causes oscillations in the solution to grow exponentially and likely causes the solver to produce unreliable results. This is the case even if only one element is smaller than what the chosen time step allows.

#### 2.2.3.1 Mesh quality

The quality of a mesh can be assessed through various criteria, including the evaluation of the geometric shapes of elements in comparison to the element's ideal shapes. By evaluating the elements contained in the mesh, the elements with poor quality are identified and thereafter improved. The mesh quality parameters of interest in this project encompass Aspect ratio, Jacobian, as well as pure geometric parameters including negative volume, minimum and maximum lengths, and angles. These parameters collectively provide insights into the overall quality and robustness of the mesh, guiding the assessment and refinement process. The quality parameter for the aspect ratio is defined as the ratio between the longest and shortest edge [12]. The Jacobian is a value between 0 and 1, it represents how much the element deviates from the ideal geometric shape of the used element [13]. A value of 1 indicates an ideal shape. The determinant of the Jacobian element quantifies the extent of local deformation required to map the parametric space onto the global coordinate system.

#### 2.2.3.2 Hourglassing and shear locking

An important aspect of the mesh is the element type used and problems that can arise using it. To obtain a reliable result, phenomena like hourglassing and shear locking need to be avoided. Hourglassing can occur in first order elements using a single integration point called reduced integration. Hourglassing essentially means that elements can deform without strain, yielding unphysical results [14]. The elements typically take an hourglass shape after such a deformation, hence the name. A sketch of the phenomenon can be seen in Figure 2.4. This issue can for example be mitigated by using second order elements.

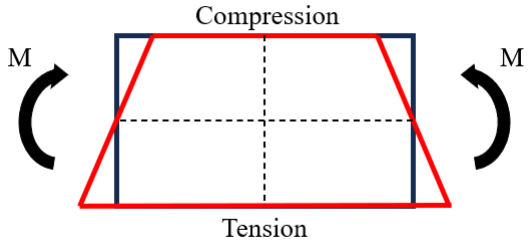


**Figure 2.4:** Sketch of an element subjected to hourglassing.

Shear locking can occur in first order fully integrated elements in bending. If the elements edges are unable to bend, a nonphysical shear strain appears, and the elements may be too stiff to use in bending dominated problem. This issue can also be reduced using second order elements [14].

#### 2.2.3.3 Element type

The elements used in the project are hexahedral brick elements of the first order, wedge elements and second-order tetrahedral elements. The brick elements have an equivalent shape of a cube and have 8 nodes, 1 at each corner. These elements are called C3D8R in ABAQUS. The wedge elements are extruded linear triangles with a total of 6 nodes, C3D6. The elements used the most are tetrahedral elements, C3D10M. These are 10-node quadratic tetrahedral elements. The C in the name stands for continuum stress/displacement [15], which means that this element is suited for displacement and/or stress analysis. 3D means that the element is 3-dimensional and the number indicates how many nodes the element has. Lastly, some element has a letter at the end of the name, this letter (R) or (M) indicates if the element has reduced integration points or if it is modified.

The elements that can use a reduced integration scheme, (R), are quadrilateral and hexahedral elements [16]. All wedge, tetrahedral and triangular solid elements utilize a full integration scheme. However, elements with different integration schemes can still be used in the same mesh. Reduced-integration elements utilize one less integration point in each direction compared to fully integrated elements. In the case of reduced-integration linear elements, a single integration point is situated at the centroid of the element. Modified elements, (M), are applicable for triangular and tetahedral elements [15]. These elements operate well when the element interacts and they demonstrate minimal shear and volumetric locking. Modified triangular and tetrahedral elements are stable under finite deformation.

## 2.3 Analysis output

There are different ways to retrieve the results from an analysis. In an explicit analysis, most of the system's progression during loading, deformation and reaction are

often of interest.

When defining the output for such an analysis, the problem at hand needs to be considered. Specifically, the time duration for the simulation and the frequency of the oscillation of different parameters are important to fully capture the behaviour of the system. For example, if the system's displacement changes or oscillates once every second, an output from the analysis needs to occur more frequently than once every second to capture the response. To fully capture the behaviour the output needs to occur much more frequently. The output frequency can either be found by investigating the analysis result using different output frequencies until convergence is found, or by using test data from the same, or a similar system that is to be modeled.

## 2.4 Data signal filter

A filter is used on data to suppress unwanted features of a signal, for example, noise or data readings caused by a phenomenon that is not of interest. A filter can be both analogue and digital. Two examples are lowpass-, and bandpass filters. A lowpass filter attenuates high frequencies while a bandpass filter only shows frequencies in a specific range [17].

A digital filter uses a cutoff frequency and a mathematical order of the filter. The cutoff frequency specifies at which frequency the filter will no longer pass a signal. The order is the degree of approximating the mathematical polynomial. Higher order brings the filter closer to an ideal response [17]. Filters can also add delay to the signal, which is known as a phase shift. The signal is then shifted a number of degrees before or after the input signal.

When the empirical data for this project was collected, a Bessel filter was used to process the data. A Bessel filter is a filter which preserves the wave shape and is designed to keep a maximally linear phase response.

## 2.5 Multivariate regression

Multivariate regression analysis is a statistical method used to investigate the relationship between multiple explanatory variables ($X_n$) and a single response variable (Y) [18]. In this project, a linear regression model is employed. Linear regression is used to estimate the coefficients of a linear equation that best fits the relationship between the independent variables and the dependent variable. The regression equation represents the relationship between the dependent and independent variables, as shown in Equation (2.4).

$$Y = \beta_0 + \beta_1 X_1 + +\beta_2 X_2 + ... + \beta_n X_n + e \tag{2.4}$$

$Y$ is the response variable, $\beta_0$ the interception, $\beta_1, \beta_2, ....\beta_n$ are the coefficients of the explanatory variables and $e$ is the error term. The error term is assumed to have a

mean of zero [19].

The output of the regression is a regression statistics table and a regression coefficient table. The content of these are shown below.

### 2.5.1 Regression statistics table

The regression statistics table consist of the following parameters [20]:

- Multiple R - A correlation coefficient that measures the strength and direction of the linear relationship between the response variable and the explanatory variables. It ranges from 0 to 1, with higher values indicating a stronger relationship and better fit of the regression model to the data.
- R square - The coefficient of determination. It represents the proportion of the variance in the response variable that is accounted for by the explanatory variables. It ranges from 0 to 1 where 1 is a perfect fit.
- Adjusted R Square - Used when the number of explanatory variables increase, a modified version of R Square.
- Standard error - The estimated standard deviation of the error ($e$).
- Observations - Number of observations used in the regression.

### 2.5.2 Regression coefficient table

A regression coefficient table shows the output of the regression for each explanatory variable and the intercept. The parameters to analyse are;

- Coefficient - Gives the least square estimation of each coefficient of the explanatory variables.
- Standard error - The standard error associated with each coefficient estimation.

- t Stat - A measure of the significance of the coefficient estimate. Higher values indicate a higher importance of the coefficient.
- P value - Low values (below 0.05) concludes into that the group is statistically significant.
- Lower 95% - Defines a lower 95% confidence interval for each coefficient estimate.
- Upper 95% - Defines an upper 95% confidence interval for each coefficient estimate.

# 3
# Methodology

The methodology of the project is presented below. This chapter explains the different methods used, as well as the workflow. Starting from the overall approach and simulation strategy, down to the establishment and execution of the computational setup, and concluding with the post-processing of results. A flowchart of the simulation workflow of the project can be seen in Figure 3.1. Furthermore, a regression was constructed to predict the strain from the teeth strokes during the gear change.

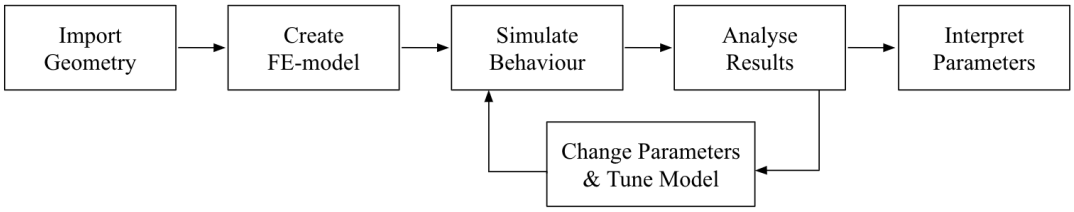


**Figure 3.1:** Flowchart displaying the overall methodology of the simulations of the project.

## 3.1 Used software products

In order to create the model, process the given empirical test data and analyse the results, different computer software were used. Figure 3.2 gives an overview of how the different programs have been used, which are also detailed below.

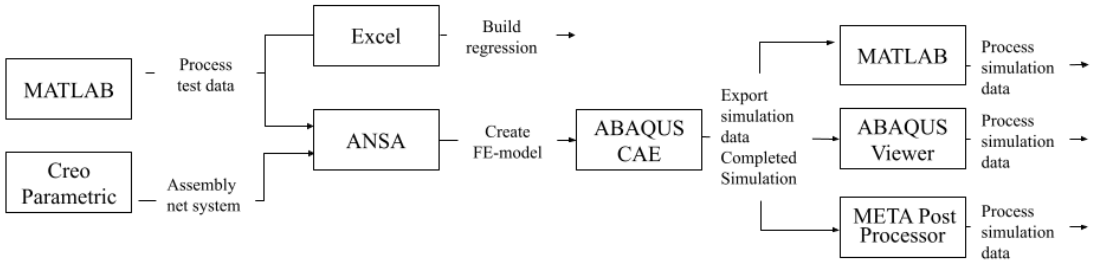


**Figure 3.2:** Overview of the different software used in the project.

**MATLAB**. A commercial software used for numerical computations. The program was used to process the given test data and for comparisons between the simulation data from ABAQUS CAE and test data.
**Creo Parametric**. A commercial software for 3D CAD modelling. The program was used for assembling the geometry.
**ANSA**. A commercial multifaceted CAE pre-processing software. It was used to create the FE model based on the imported 3D assembly.
**ABAQUS CAE**. A commercial FE software. Was used for solving the FE model created in ANSA.
**ABAQUS Viewer**. A commercial software for post-processing. The program was used to view and extract the results provided by the FE-solver.
**META Post Processor**. A commercial software for post-processing. The software was used to extrude strain data from simulation results.
**Microsoft Excel**. A commercial spreadsheet program which has been used to store data as well as for building a multivariate regression.

## 3.2 CAD

The Finite Element model was created using the provided 3D CAD models, which outlined the geometry of the rod, shift fork, ring gear, and pads. Some models were adjusted to simplify the geometry and to closely resemble the used parts in the tests. All CAD models were provided by Volvo GTT.

### 3.2.1 Rod

Figure 3.3 shows the CAD model of the rod. The rod is moved by a pneumatic cylinder that pushes the rod which in turn transports parts through the gear shift. The rod is attached to the shift fork and the transmission housing. The rod is longer in the real AMT and is attached to the pneumatic cylinder, but the simulations only require the shown part of the rod.

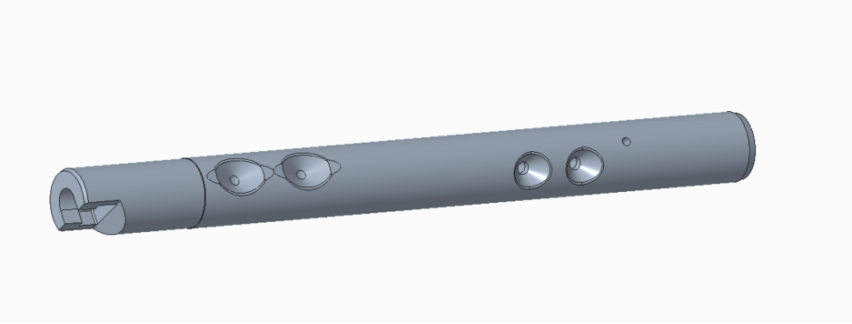

**Figure 3.3:** CAD model of the shift rod.

### 3.2.2 Shift fork and pads

The shift fork together with the brass pads, used to reduce sliding friction, is illustrated in Figure 3.4. This CAD model was altered from the original CAD model

since the tests were performed with a shift fork that has been machined, in order to attach strain gauges for testing. The pads were not modified in any way at this stage of the project. The pads can be seen attached to the bottom of each arm on the shift fork.

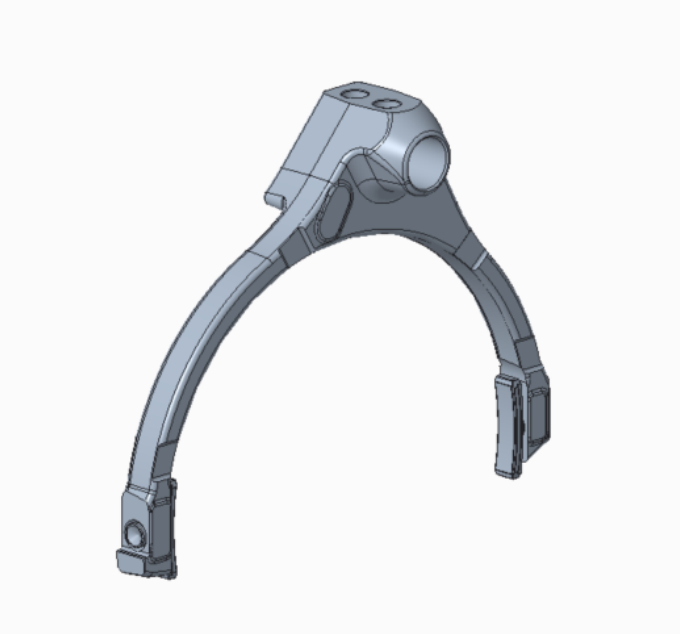

**Figure 3.4:** CAD model of the machined shift fork together with the pads.

### 3.2.3 Ring gear

The ring gear, depicted in Figure 3.5, underwent modifications aimed at simplifying its geometry, thereby reducing simulation time. This involved eliminating complex shapes, such as the gear teeth, to improve computational efficiency.

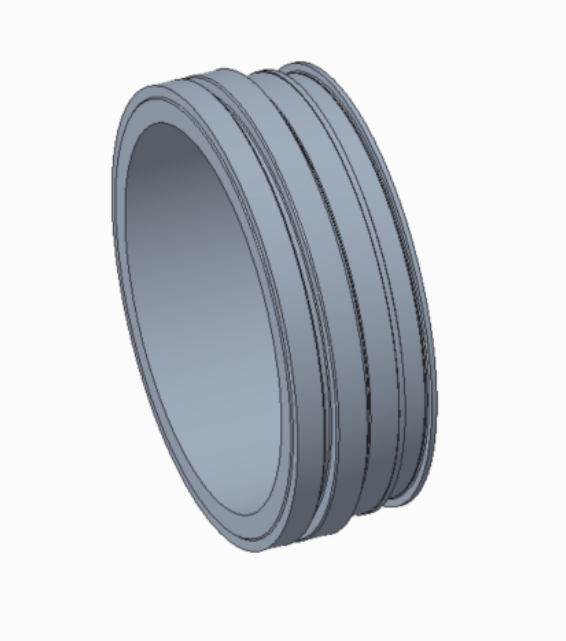

**Figure 3.5:** CAD model of the modified ring gear. Note that the gear teeth have been removed from the model.

### 3.2.4 Housings

The used housings in the model, the parts that hold up the rod, are created directly in ANSA. The methodology for this procedure was to extrude a defined surface. The surface was defined by creating 2 nodes for each house and then create a closed surface between the node pairs. The surface were then meshed with a structural second order quad mesh, and extruded to turn the surface into a volume. By using this method, the housings fit perfectly to the rod. Already existing housings, provided by Volvo GTT, could be used but the advantage of this method is the reduction of elements and avoiding problems with the mesh quality.

Lastly, all parts were assembled using Creo. The entire assembly is shown in Figure 3.6.

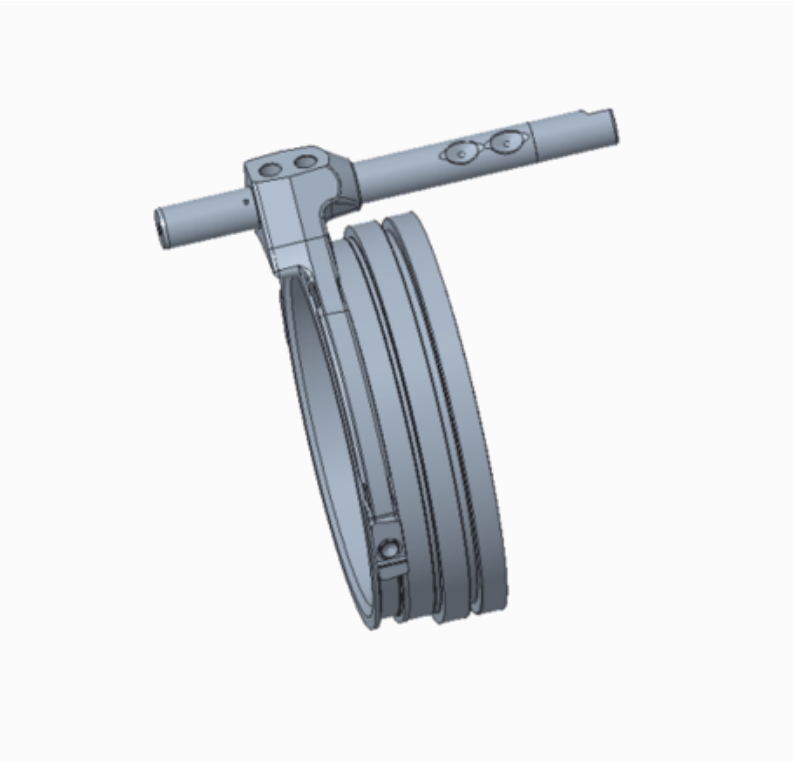

**Figure 3.6:** CAD model of the assembly.

## 3.3 Test data

Data from physical testing of the transmission has been provided. This data includes: the position, net force, velocity and acceleration of the rod; strain from 3 strain gauges on the fork; as well as rotational speed differences in the system. This data has been collected from a variation of different types of shifts, where rotational speed, ambient oil temperature, low to high shift or high to low shift are varied. In this project, 30 cases have been analysed and used.

### 3.3.1 Determine rod, fork and ring gear position

The position of the rod is given in the test data. The ring gears position is not measured, but due to the ring gear first making contact with the housing, its position is also important when correlating the model results to the test data. Thus, this position needs to be calculated.

This is done by finding the difference in the position of the rod in its loaded end state in one shift and its unloaded start state in a shift in the opposite direction. Hence, the position of the rod for when the gear goes from high to low and then back to high for testing with the same external circumstances, the identical case of shift but with opposite gears. By taking this difference in rod position and dividing by the strain in the fork in the end position, and then multiplying with the strain over the entire time duration, the position of the fork is found. To then get the ring

position, the fork position is simply added to the position of the rod. The equations are shown below in Equations (3.1) and (3.2).

$$\delta \underline{u}_{\text{Fork}} = \frac{\delta u_{\text{rod,end}}}{\varepsilon_{\text{end}}} \cdot \underline{\varepsilon} \tag{3.1}$$

$$\text{Pos}_{\text{Ring}} = \text{Pos}_{\text{Rod}} + \delta \underline{u}_{\text{Fork}} \tag{3.2}$$

In the equations, $\delta \underline{u}$ is displacement and $\underline{\varepsilon}$ is strain. Vectors are underlined.

### 3.3.2 Determine ring gear velocity

To find the velocity of the ring gear over time, the time derivative of the position vector is calculated. To be able to use this data, the velocity must be filtered in the same way as the velocity data for the rod. The filter used is a zero phase shift second order lowpass Bessel filter with a cutoff frequency of 800 Hz. It is the same filter that is used when collecting the empirical data. After filtration, the impact velocity of both the ring gear and the rod can be found. The position graph is studied to find at what time the impact occurs on the ring gear. This point in time is then transferred to the velocity graph, where the velocities will be approximately 0. It is then assumed that the impact velocity is equal to the maximum absolute velocity just prior to the impact. This estimation corresponds to a worst-case scenario since it will impact with the highest recorded velocity in the time frame, and thus be on the safe side.

### 3.3.3 Strain data

The strain measurements comes from 2 half bridge strain gauges and 1 full bridge strain gauge. The position of the strain gauges are shown in Figure 3.7. The double arrows on the fork arms indicate the direction of the strain gauges. The figure illustrates the geometry after it has been meshed, which gives the geometrical irregularities.

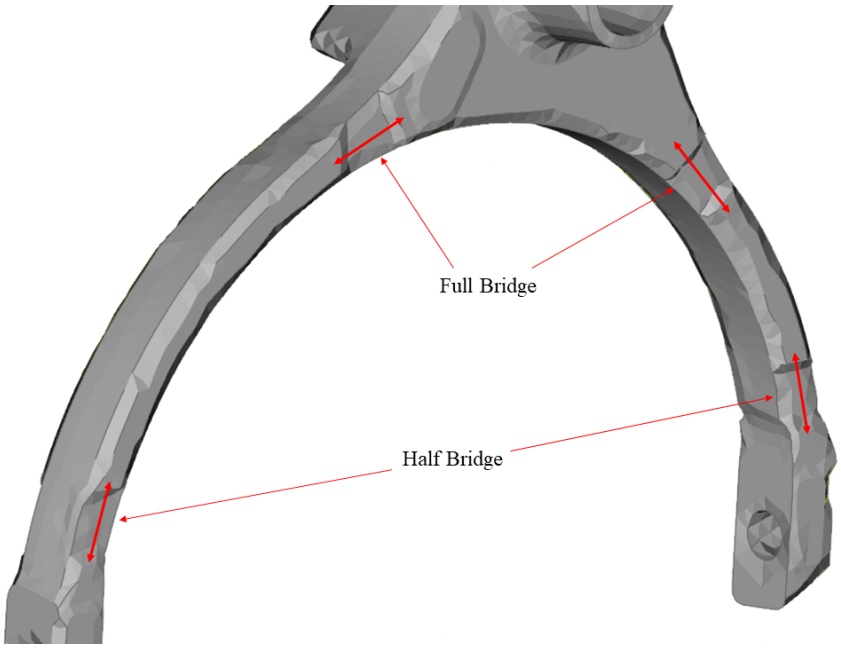


**Figure 3.7:** Strain gauge positions on the shift fork after it has been meshed.

The half bridge strain gauges are placed on each arm of the fork and consist of a sensor on each side of each arm. The full bridge is placed higher up on the fork, and consist of 4 sensors.

## 3.4 The finite element model

This sub-section outlines the procedure used to characterize the gear changes as a finite element simulation. Employing the graphical interface in ANSA, the Finite Element models were defined and configured to be calculated in ABAQUS.

### 3.4.1 Defining part identities

The CAD assembly file was imported into ANSA as an STP-file. Due to the diverse mesh requirements for different parts and sections of the model, including variations in element type and material, the domain was subdivided into distinct properties, each associated with a specific Part Identification (PID) with its own colour coding. In Figure 3.8a, an overview of PID distribution is presented, with definitions for each PID provided in Figure 3.8b. The usage of PIDs facilitates the meshing procedure since each PID can be meshed at a time. PIDs also offer more options when defining boundary conditions and initial conditions.

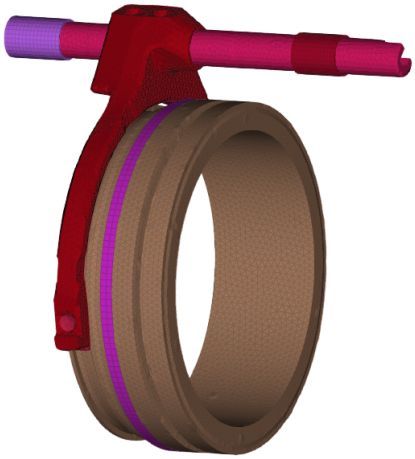

| Id | Name | PID |
|---|---|---|
| 1 | Extruded Wall | 1 |
| 2 | Machined Yoke Volume | 2 |
| 3 | Pad Volume-L | 3 |
| 4 | Ring Gear Volume | 4 |
| 5 | Rod Volume | 5 |
| 6 | Pad Volume-R | 6 |
| 7 | Bearing_Front_New | 7 |
| 8 | Bearing_Back_New | 8 |

**Figure 3.8:** Colour coded PIDs (a) with corresponding list from ANSA (b).

### 3.4.2 Meshing procedure and used element formulation

To mesh the model, a combination of shell and solid elements has been used. First, the parts are meshed with shell elements which then are turned into solid elements. Each PID has been meshed individually and manually to control the mesh structure of each geometry. This method has allowed for an approach where small, inessential geometrical details have been disregarded due to that they will not substantially alter the response. In general, a coarse mesh has been used with a length of 5 mm for each shell element. The PIDs have also been altered since some surfaces are irregular or include features that are not important for the purpose of the project. These areas have had elements which have not fulfilled the mesh quality criteria threshold values chosen which lead to modifications in the shell mesh. The quality criteria threshold values can be seen in Table 3.2.

The parts were firstly modelled with triangular shell elements. When creating the shell mesh, some features of the rod were deleted. The rod model originally had a hole for airflow which was removed since this feature is irrelevant for the project. Other geometry details modified were surface smoothing and the removal of the immersions for the spring-loaded detent which is a gear-shift control. Further, the rod was then modelled with tetrahedral volume elements, by extruding the triangular shell elements. The fork was modified by smoothing out some surfaces involving fillets and level differences. The fork was initially meshed with triangular shell elements and later with tetrahedral volume elements. The pads had many fillets which led to further surface smoothing. The pads were initially meshed using triangular shell elements, and subsequently, tetrahedral elements were employed as volume elements. The ring gear was also modelled using triangular shell elements and tetrahedral volume elements. Moreover, the housings are modelled using hexahedrons and the extruded wall is modelled with pentahedral elements.

The housings are modelled in C3D8R elements. The Extruded wall is modelled

with six-node triangular prism elements. The remaining parts are modelled using C3D10M elements. All volume element shapes, types and the amount of solids elements are summarised in Table 3.1. After the shell elements have been used to create the volume elements, they are disregarded.

| Part | Element Shape | Element Type | Number of Elements |
|---|---|---|---|
| Rod | Tetrahedral | C3D10M | 21 034 |
| Ring Gear | Tetrahedral | C3D10M | 75 411 |
| Fork | Tetrahedral | C3D10M | 22 101 |
| Pads | Tetrahedral | C3D10M | 2 132 |
| Housings | Hexahedral | C3D8R | 810 |
| Extruded wall | Pentahedral | C3D6 | 1 332 |

**Table 3.1:** The used element shape, type and number of solid elements for each part.

| Element Type | Quality parameter | Value |
|---|---|---|
| Shell | Aspect | 3 |
| - | Jacobian | 0.7 |
| - | Negative Volume | Partial |
| - | Min. Length | 1.8 mm |
| - | Angle Min Tetras | 20 |
| - | Angle Max Tetras | 120° |
| Volume | Aspect | 3° |
| - | Jacobian | 0.7 |
| - | Negative Volume | Partial |
| - | Min. Length | 1.8 mm |
| - | Angle Min Tetras | 20° |
| - | Angle Max Tetras | 120° |

**Table 3.2:** Mesh criteria for shell and solid elements.

### 3.4.3 Material definitions

The simulation model incorporates five different materials, all assumed to exhibit isotropic behaviour. These materials include brass, steel, forged steel, aluminium and lastly a rigid material chosen to replicate the impact surface when the fork strikes the extruded wall in the simulation. Table 3.3 lists the material parameters assigned to each of these materials used throughout the simulations. Table 3.4 provides a list of each analysed part, accompanied by its respective material.

| **Material name** | **Young's modulus** $E$ [GPa] | **Density,** $\rho$ $[\frac{\text{kg}}{\text{mm}^3}]$ | **Poisson's ratio** $\nu$ [ ] |
|---|---|---|---|
| Steel | 200 | 7.85 | 0.300 |
| Forged steel | 210 | 7.85 | 0.300 |
| Brass | 125 | 8.4 | 0.330 |
| Aluminum | 74 | 2.75 | 0.389 |
| Rigid material | 10 000 | 1 000 | 0.300 |

**Table 3.3:** Material properties in the FE model.

| **Part** | **Material name** |
|---|---|
| Rod | Steel |
| Ring Gear | Steel |
| Shift fork | Forged steel |
| Pads | Brass |
| Housings | Aluminum |
| Extruded wall | Rigid material |

**Table 3.4:** Parts and their assigned material.

### 3.4.4 Constraints

To apply the required boundary conditions and loads for the simulation, kinematic couplings (*COUPLING, CONSTRAINT) are employed, as illustrated in Figure 3.9. These couplings constrain the movement of coupled nodes on the solid mesh to synchronize with the rigid body motion of the reference node. The reference node is the master node meanwhile all other nodes connected to the coupling are slave nodes. The slave nodes DOF are constrained relative to the reference node, the master node. Meaning that the slave nodes move in relationship to the master node.

The blue lines in the figure show the coupling between the nodes. Two distinct couplings are utilized: Coupling 1 restricts all slave node's degrees of freedom to the master node while Coupling 2 locks all slave node's degrees of freedom to the master node except the translational degree of freedom in the $z$-axis. Both loads and boundary conditions are imposed on these couplings.

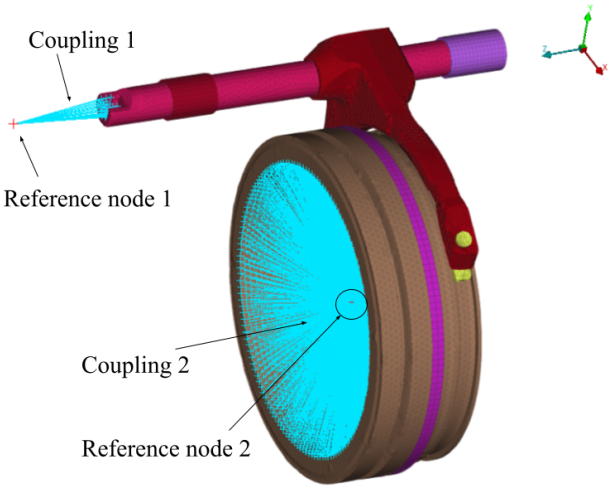


**Figure 3.9:** Figure from ANSA displaying the locations of the two couplings in the model with the corresponding reference node.

#### 3.4.4.1 Loads and mass

Coupling 1 is loaded by an axial force in the reference node to propel the rod during the shift. The node, in which the kinematic coupling is defined, is also defined with a mass of 0.5 kg to replicate the extension of the rod. The load in the axial direction is a net force from the forces remaining in the system, that varies in each gear change, based on the test data, in ANSA applied as a concentrated load (*CLOAD).

#### 3.4.4.2 Spring

The previously mentioned axial force originates from the pressurised cylinder connected to the rod. Given the nature of pressure, the load decreases as the cylinder volume increases due to the movement of the rod. To capture this in the model, a spring is used. The spring is connected in the same node as the force, which means that it will create a force acting opposite the applied axial force as the rod translates. The spring will further help damp out oscillations after the gear shift is complete. The spring constant is set to 775 $\frac{\text{N}}{\text{mm}}$. The spring constant is calculated based on the net force from the pressurised cylinder and the displacement of the rod at the end of the shift sequence found in the test data. It is assumed that the pressure curve can be approximated as linear using a spring element. The pressure curve is displayed in Figure 3.10.

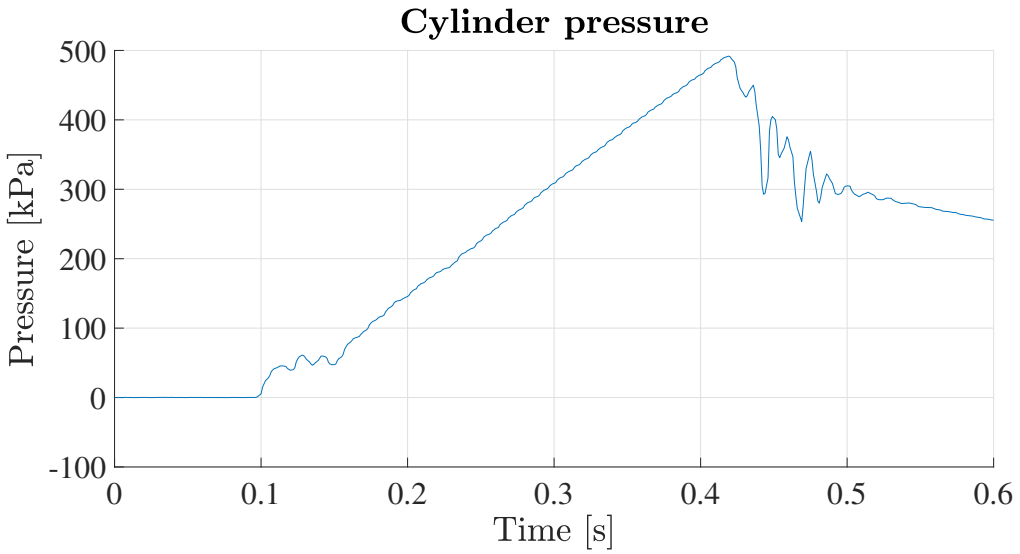


**Figure 3.10:** Pressure curve based on the empirical test data used to calculate the spring constant.

The spring element used in ANSA (*ELEMENT, TYPE=SPRINGA) is set up in two different nodes. The main node is the reference node for Coupling 1. The second node is offset from the reference node which in turn is locked in all degrees of freedom, the spring is depicted in Figure 3.11.

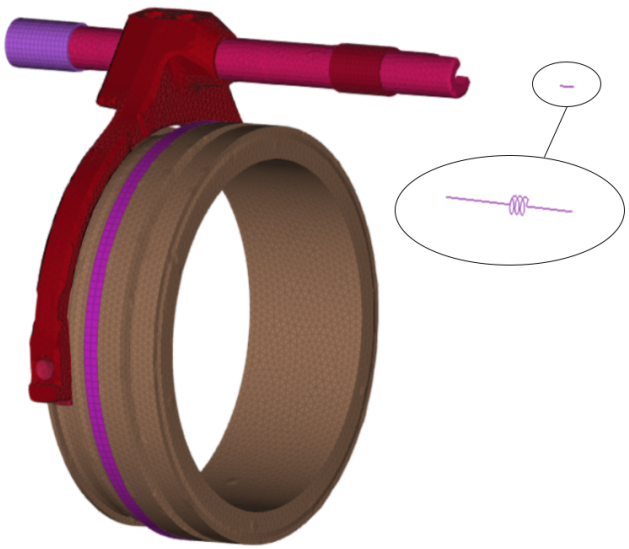

**Figure 3.11:** An enlarged figure of the spring connected to the rod.

#### 3.4.4.3 Boundary conditions

The boundary conditions in the models are as follows, the housings are locked in all DOFs. They are locked by defining a set on the outside surface of each house and then locking its DOFs. The end node of the spring is locked in all DOF. The ring

gear is free to move in the $z$-translational axis. The extruded wall is constrained in all translational DOFs. The Boundary conditions are displayed in Figure 3.12 and explained in Table 3.5.

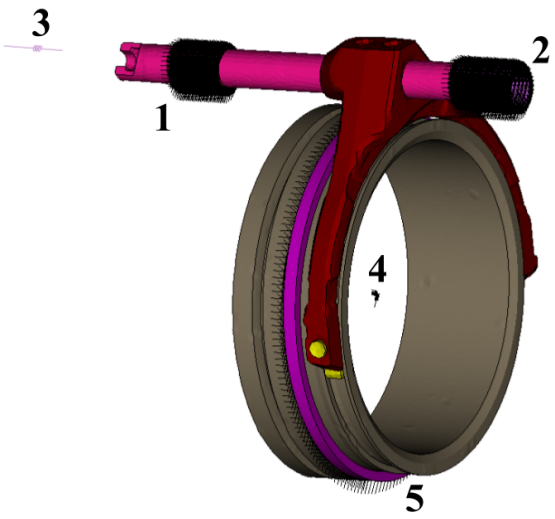


**Figure 3.12:** Figure from META Post Processor displaying the locations of the boundary conditions in the model.

| | Coupling | Locked Degree of Freedom |
|---|---|---|
| 1 | Housing | 123456 |
| 2 | Housing | 123456 |
| 3 | Spring-node | 123456 |
| 4 | Ring Gear | 12456 |
| 5 | Extruded wall | 123 |

**Table 3.5:** The constraints applied to the FE model. DOF 123 mean translational xyz-direction, while 456 mean rotational xyz-direction respectively.

#### 3.4.4.4 Damping

The damping in the model was modelled using Rayleigh damping, as described in Section 2.2.2. The model has a relative damping ratio, $\zeta$, of 6% and the damping ratio was estimated by finding the natural frequency from the test data, by analysing the displacement plot of the rod. The frequency was estimated to 120 Hz and then converted from frequency to angular velocity. Moreover, the calculation can be seen in Equation (3.3).

$$\alpha = 2\omega\zeta = 2(120 \times 2\pi) \times 0.06 = 90 \tag{3.3}$$

Here, $\beta = 0$, since a non-zero value resulted in numerical instability. The stiffness coefficient, $\alpha$, was then applied for each of the materials in ANSA.

### 3.4.5 Initial conditions

An initial velocity is assigned to all movable components in the simulation, including the rod, shift fork, pads, and ring gear. This velocity changes during the shift and for different recorded shifts, therefore will this be a parameter throughout the project in order to emulate the given test data. As the ring and rod does not move in unison, the velocity used in the simulation is a weighted average velocity of the rod and the ring gear based on the weight of all of the moving components.

To confirm that the weighted velocity used is representative, scatter plots of the different velocities against the displacement of the rod in different stages of the oscillations are created. The velocities compared are the velocity of the rod, ring gear and the weighted velocity against the comparison in displacement for the first oscillation for the rod.

An investigation into using 3 different velocities was also conducted. The velocities were the known rod and ring gear velocities meanwhile the third velocity was an average value of the known velocities applied on the fork. A comparison of using 1 or 3 velocities was done for selected cases. In total, 10 different cases were compared. The results are presented in Section 4.2.2.

### 3.4.6 Contact definitions

The FE simulation requires different kinds of contacts. The contacts are applied between all the different parts. In this simulation, the contact definitions used are Tie (*Tie) and Contact pair (*Contact Pair). The tie is between the fork and the rod meanwhile all other contacts are designated as Contact pairs. See Figure 3.13 for clarification on where all contacts are placed. There are a total of 16 contacts used in the model, each pad has a total of six contact definitions.

Contacts 7 and 9 are on each side of the pads and they interact with the ring gear. Contacts 6 and 10 interact on the back side of the pad with the fork. Contact 8 connects the target surface of the pad to the ring gear and contact 5 connects the pad to the fork. See Figures 3.13a and 3.13b.

With the exception of the contacts between the housings and the rod, as well as the contact between the ring gear and the extruded wall, all contacts embody a frictional component. The friction coefficient remains unknown, prompting the selection of a conservative value, set at 0.05. Hence, the contacts involving the housings and rod, as well as the ring gear and the extruded wall, are frictionless. All contacts are of the type Type=NODE TO SURFACE, see Table 3.6 for a summary of the contacts.

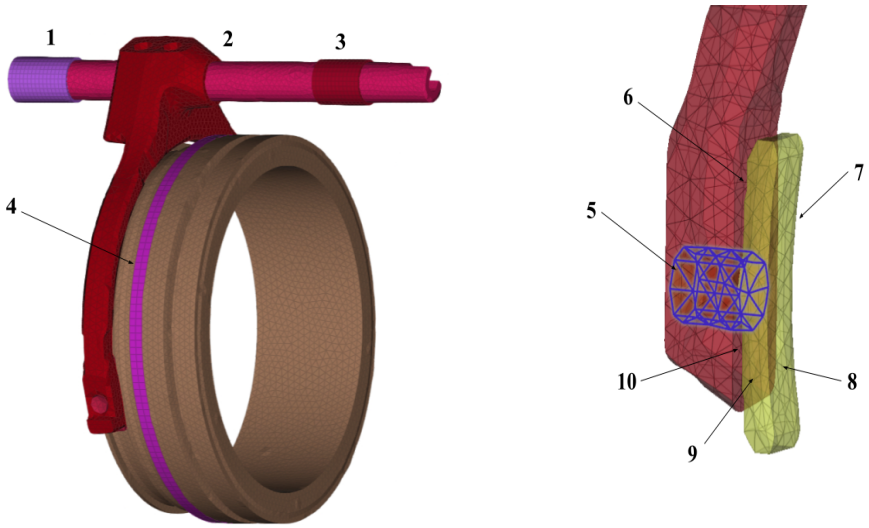


**(a)** Contacts defined in the model. **(b)** Contacts defined on the pads.

**Figure 3.13:** All contacts in the model.

| Name | Definition | Friction, $\mu$ | Type |
|---|---|---|---|
| 1. Rod to Housing Back | Pair | 0 | Node to Surface |
| 2. Rod to Fork | Tie | - | Node to Surface |
| 3. Rod to Housing Front | Pair | 0 | Node to Surface |
| 4. Ring Gear to Extruded Wall | Pair | 0 | Node to Surface |
| 5. Pad to Fork | Pair | 0.05 | Node to Surface |
| 6. Pad to Fork | Pair | 0.05 | Node to Surface |
| 7. Pad to Ring Gear | Pair | 0.05 | Node to Surface |
| 8. Pad to Ring Gear | Pair | 0.05 | Node to Surface |
| 9. Pad to Ring Gear | Pair | 0.05 | Node to Surface |
| 10. Pad to Fork | Pair | 0.05 | Node to Surface |

**Table 3.6:** Detailed summary of the contact properties in the model.

## 3.5 Dynamic simulation

To tune the FE model based on the provided empirical test data. The simulation focused on replicating the concluding phase of the shift change, specifically the moment when the fork reaches the end wall. The test data first compared with the test data was the displacement of the fork. Later, when the FE model recreated the behaviour seen in the telemetry, the strain was analysed. The second step was to simulate the tooth clash between the housing and the ring gear, which can occur during a shift. Due to the simplicity of the built FE model, a multivariate regression was instead made to estimate the teeth hit, which can be seen in Section 3.6. The model isn't built to consider the different kinds of hits that can occur during the gear exchange, especially the angle at which the hit occurs can cause rotations. The

model only considers axial displacement and not rotations.

### 3.5.1 Simulated end-stop impact

The simulation focused on the part of the gear change where the fork reaches its final position when it goes from high-range gear into low-range gear. To simulate this final step of the gear exchange, an extruded wall has been used. The wall is an offset extrusion from one of the flat surfaces on the ring gear. The wall's purpose is to replicate when the engaging sleeve hits the gear wheel and the tooth clutch engages. The extruded wall can be seen in Figure 3.13 as a purple section in connection to the ring gear. In order to replicate the test data, some kind of damping had to be used to reduce the displacement oscillations after the hit. Hence, contact damping was used to replicate energy lost from deflections of the housing.

The methodology for finding an illustrative value for the contact damping, in the contact between the extruded wall and the ring gear was an iterative approach. Different values were tested and based on the already motivated parameters from the test data and calculations, as the spring stiffness, the concentrated force and the initial velocity of the system, a contact damping of 0.05 was chosen.

## 3.6 Multivariate regression

The last step in the project was to investigate a shift where the teeth in the ring gear and housing clash. This sequence has too many parameters to simulate. Instead, a multivariate regression analysis was performed to investigate which parameters are of importance in this collision. The model can then be used to predict the strain in the fork given a set of input parameters. This is under the assumption that the shift fork strains can be replicated in the simplified model by tuning the initial conditions.

The parameters of the regression model are found from the provided empirical data. The used scalar values are extracted from the time instant when the ring gear teeth impact the housing. The independent variable is the strain in the full bridge, and the dependent variables are listed below:

- Ring velocity
- Ring acceleration
- Rod velocity
- Rod acceleration
- Main shaft rotational velocity
- Output shaft rotational velocity
- Net force from the pneumatic cylinder acting on the rod

- Axial position of the ring when the gear teeth clash

The regression is created using the Analysis ToolPak in Excel.

### 3.6.1 End-stop collision

An additional regression is also created for the end-stop collision, where there is no clash between the gear teeth. This is because both are required to construct a load collective. For the end-stop collision, the following variables are used:

- Ring velocity squared
- Rod velocity squared
- Ring acceleration

The squared velocities have been selected since they should describe the energy of the system at impact, and the acceleration should describe the general movement of the system.

## 3.7 Method for post-process and data organisation

The different parameters studied alongside multiple gear exchanges yielded a substantial amount of data which needed to be post-processed, compared and analysed. The primary tool for handling this data was MATLAB. A script was developed to streamline data management and ensure consistent handling and extraction of data for each gear change and simulation. The script enabled for analysis and extraction of the following empirical data from each gear change:

- Displacement, velocity and acceleration for the rod
- Displacement, velocity and acceleration of the ring gear
- Displacement of the fork
- Strain data from 3 strain gauges
- Net force from the pneumatic cylinder during the shift

Further, MATLAB is used to compare empirical and simulation data while ABAQUS Viewer and META post processor are used to extract and process the simulation data. Excel was then used to gather the collected data as well as to construct the multivariant regression.

### 3.7.1 Post-processing: CAE-Software

The primary software used for post-processing the simulations has been ABAQUS Viewer, with a complementary use of META post processor. ABAQUS Viewer was utilized for analysing simulation results, particularly focusing on the system's behaviour and the displacement of the rod and ring gear. This is done by choosing

2 nodes in the mesh, 1 on the rod and 1 on the ring gear. These are chosen to be representative of the position that has been used to get the empirical data. Since the same mesh is used for all simulations, these node numbers do not need to be altered between simulations. This also allows for accurate comparisons between different simulation results. The nodes used are node number 19 323, which is located on the ring gear, and node number 23 100, which is located on the rod. The chosen nodes are displayed in Figure 3.14 as highlighted white crosses.

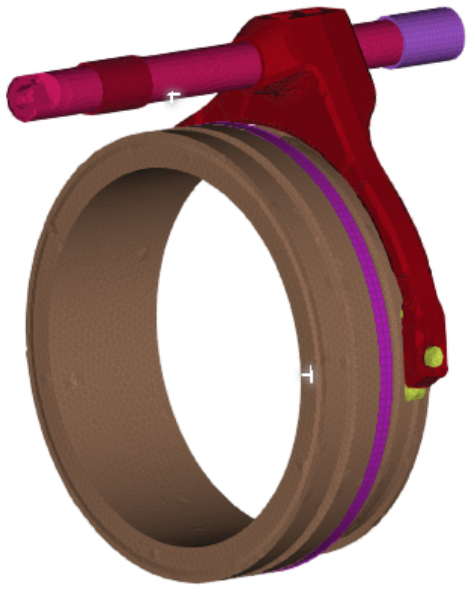

**Figure 3.14:** The data has been extracted from these highlighted nodes for the simulations.

META post processor was utilized to find the strain acting on the fork during the simulation. In META post processor, strain gauges can be applied to the geometry in the same way they were applied during the physical test model, and this provides a good basis for comparison. The META strain gauges calculate the strain between two points from the displacement. The strain gauges are set up to register the strain at 8 different points. These readings are then exported and used in calculations in MATLAB to make the readings correspond to the measured empirical strain from the 3 strain gauges.

### 3.7.2 Post-processing: MATLAB

MATLAB was utilized for retrieving and comparing data. In MATLAB, the final post-processing of the simulation results were made. The test data was imported to

MATLAB, as well as the simulation results.

MATLAB was then used for filtering of data signals, strain calculations and to create plots to evaluate and compare the test and simulation data.

### 3.7.3 Post-processing: Excel

Excel was employed to store data obtained from both simulations and test data. Subsequently, comparisons were made between the simulations and the empirical data. This stored data was then utilized to construct the regression model.

# 4
# Results

This chapter includes results produced using the methods stated in Chapter 3. The results include graphs and tables containing simulation results, test data comparisons, and the multivariate regression created. The results are further discussed in Chapter 5. Since the project has handled 30 different gear changes, all of them being unique, a selection of three cases has been made to display the results for the displacement and velocity plots. The cases selected are 5, 21 and 53. These cases are representative of all of the gear shifts since the majority of the shifts have either 1 or 2 teeth clashes. In the provided test data, the distribution of the number of teeth clashes for the shifts is as follows:

| Number of teeth hits | Quantity |
|---|---|
| 0 | 2 |
| 1 | 11 |
| 2 | 9 |
| 3 | 8 |

**Table 4.1:** The distribution of number of teeth hits per gear shift from the test data.

Case 5 has 1 clash during the gear shift, case 21 has 2 clashes and case 53 has 0 clashes. Thus, case 53 is a perfect gear change in terms of energy loss and shift time. However, more energy is carried through to the end-wall collision.

Case 21 hits the engaging sleeve distinctly twice before the tooth clutch connects fully and the shift is completed. The hits are high up on the teeth, meaning that the rebound is distinctly shown in the test data with a proportionally large rebound.

Case 5 has one clear hit, high up on the teeth before the gear shift is complete.

## 4.1 Position and velocity

The position and velocity of the ring gear have been fundamental parameters for the simulations and the multivariate regression throughout the project. The results of the displacement and velocity calculations from the empirical test data are shown below.

### 4.1.1 Position

The displacement of the rod and ring gear is shown in Figures 4.1-4.3 for the three selected cases. The red line is the calculated ring gear position, and the blue line is the rod position from the empirical test data throughout the shift process.

Figure 4.1 shows the displacement of the rod and ring gear over the whole gear change. The collision of teeth can be seen in the middle of the slope when the time is close to 0.4 s. As the figure shows, the ring gear fluctuates more compared to the rod. See Figure 4.4 for a zoomed figure on the fluctuations.

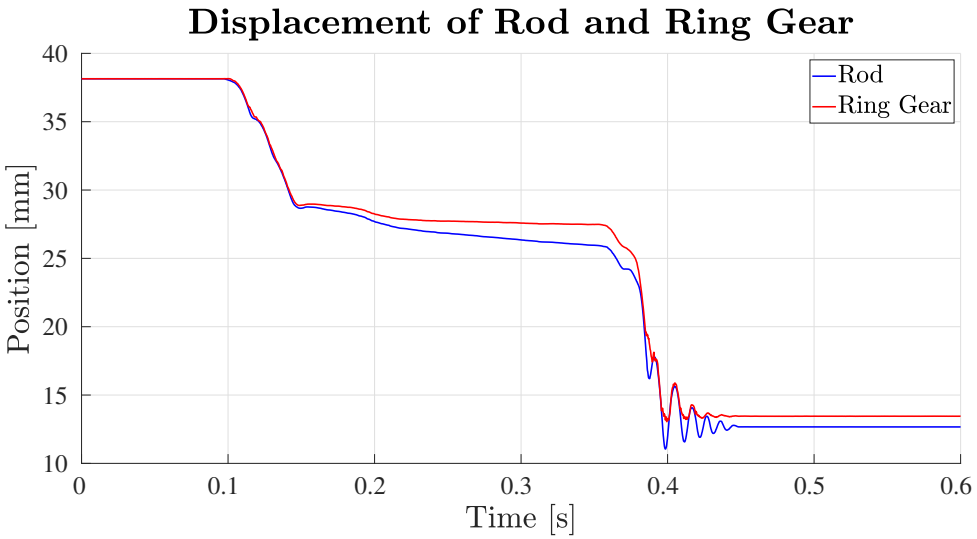


**Figure 4.1:** The displacement of the rod and ring gear for the scenario with 1 teeth collision during the tooth clutch alignment. The displacement is for the entire gear shift.

For the shift with 2 teeth collision, the displacement is shown in Figure 4.2. The first collision has a higher rebound displacement for the rod compared to the second hit, indicating that the first hit occurs higher up on the tooth than the second hit does. See Figure 4.5 for a zoomed-in section on the variation in rebound displacement between the two peaks.

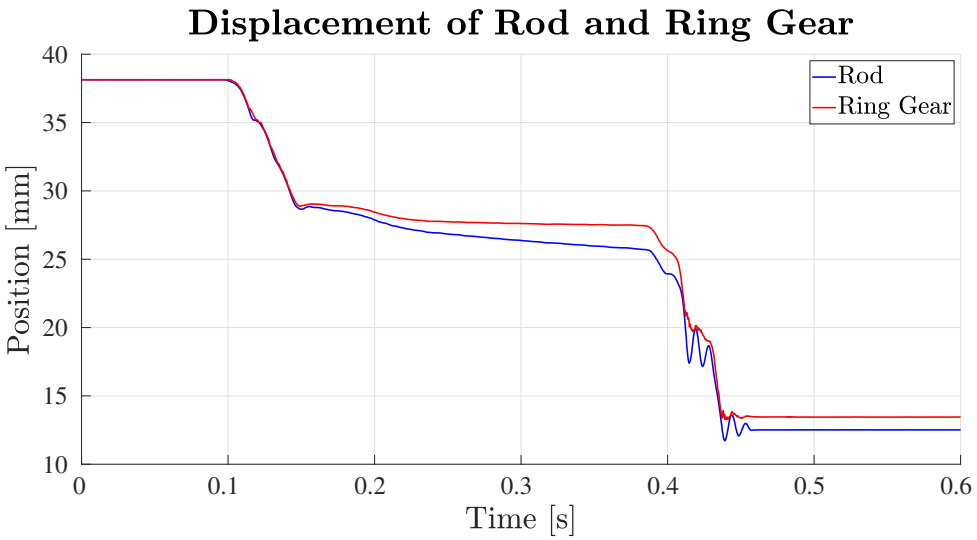


**Figure 4.2:** The displacement of the rod and ring gear for the scenario with 2 teeth collision during the tooth clutch alignment. The displacement is for the entire gear shift.

The final scenario, where no collisions between teeth occur, is shown in Figure 4.3. In this case, as there is no tooth collision during the gear change, the displacement profile exhibits a nearly continuous linear slope. The motion smoothly transitions from synchronization to engagement with no disturbances. Note the higher displacement in the rebound oscillation after the end-stop collision due to higher velocity than in the shifts with tooth collisions

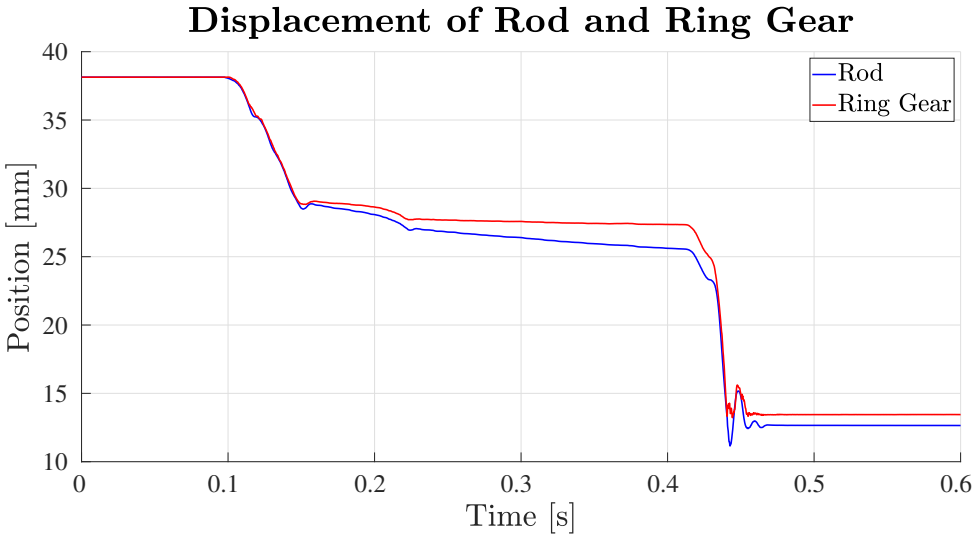


**Figure 4.3:** The displacement of the rod and ring gear for the scenario with 0 teeth collision during the tooth clutch alignment. The displacement is for the entire gear shift.

The zoomed-in figures of the fluctuations and the rebound distance are shown below. The displacement of the rod is more stable compared to the displacement of the ring

gear which fluctuates, see Figure 4.4. The trend is less stable due to the ring gear is allowed to move more freely than the rod. Another reason for the fluctuations in the ring gear is the geometry of the fork. The ring gear is attached to the fork, and the geometry of the fork is unsymmetrical. The arms of the fork have different lengths leading to arrhythmical movements and a difference in both velocity and displacement within the fork and ring gear.

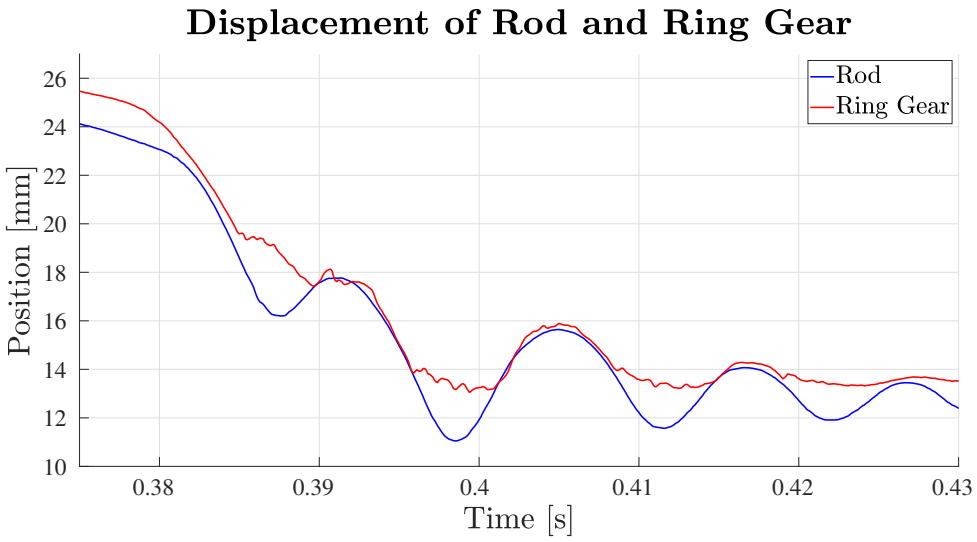


**Figure 4.4:** A zoomed in figure on the difference in fluctuations between the rod and ring gear in displacement. The scenario is taken from Case 5.

Teeth collisions can transpire at various heights along the tooth structure, either on the tooth surface or the tooth flank, the ring gear can also be blocked by the teeth. This is when it lays stationary, first unable to complete the shift. This can be seen in Figure 4.5.

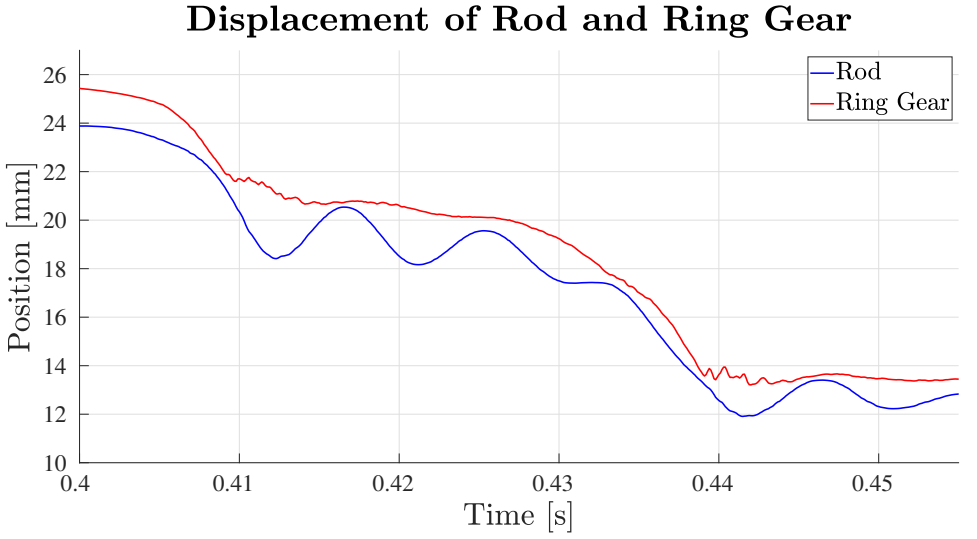


**Figure 4.5:** A zoomed figure on Figure 4.2 showing blocking of the ring gear.

### 4.1.2 Velocity

The results of the velocities are shown after being processed by a zero phase shift second order lowpass Bessel filter with a cutoff frequency of 800 Hz. The velocities of the rod and ring gear for the three selected cases are shown in Figures 4.6-4.8.

Figure 4.6 shows that the velocities for the 2 different components at the beginning of the shift process follow one another. The components are shown to correlate and be in tandem. When the teeth hit occurs, the ring gear starts to oscillate more, but the overall velocity trends for both components remain consistent, indicating continued correlation in their velocities. In general, the rod has higher magnitudes of the peaks compared to the ring gear.

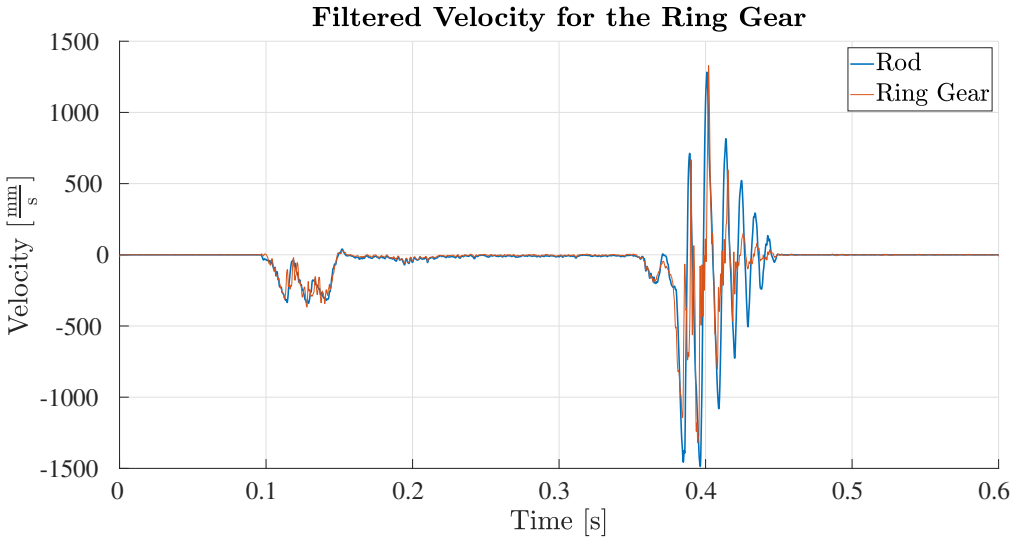


**Figure 4.6:** The velocity of the rod and ring gear for the entire shift process for case 5. The velocities have been filtered.

In Case 21, it's evident that the rod exhibits a significantly higher absolute velocity compared to the ring gear. However, the correlation between the 2 components is less pronounced in this scenario. The velocity of the ring gear shows greater fluctuation, with more rapid increases and decreases compared to the rod. The rod demonstrates longer periods of sustained velocity changes, both in terms of increases and decreases, see Figure 4.7.

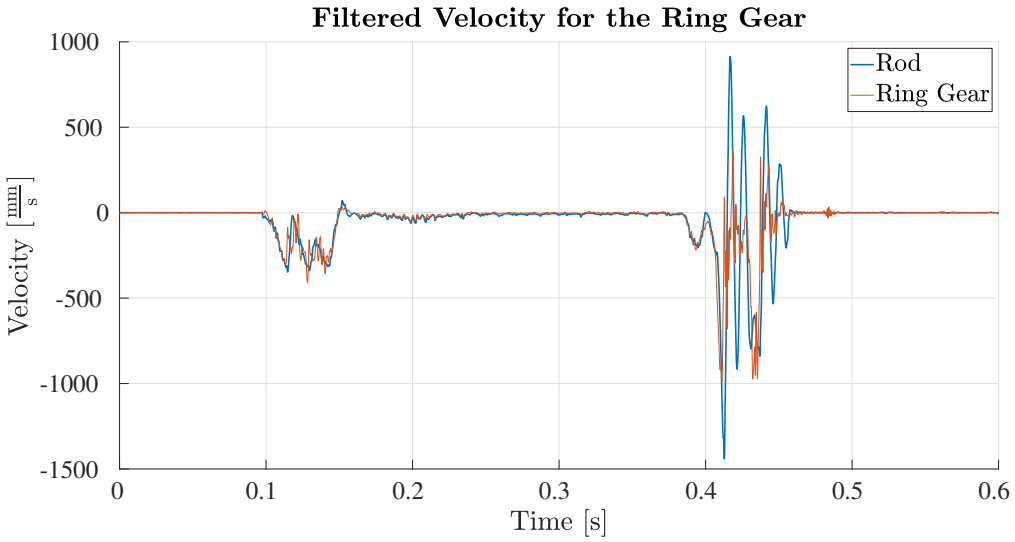


**Figure 4.7:** The velocity of the rod and ring gear for the entire shift process for case 21. The velocities have been filtered.

In the case of 0 teeth collisions, the shift process proceeds without disturbance, leading to a smoother shift. As shown in Figure 4.8, fewer velocity peaks are observed compared to cases 5 and 21. Moreover, the velocities of both the rod and ring gear are shown to follow each other, indicating a correlation between the 2 components.

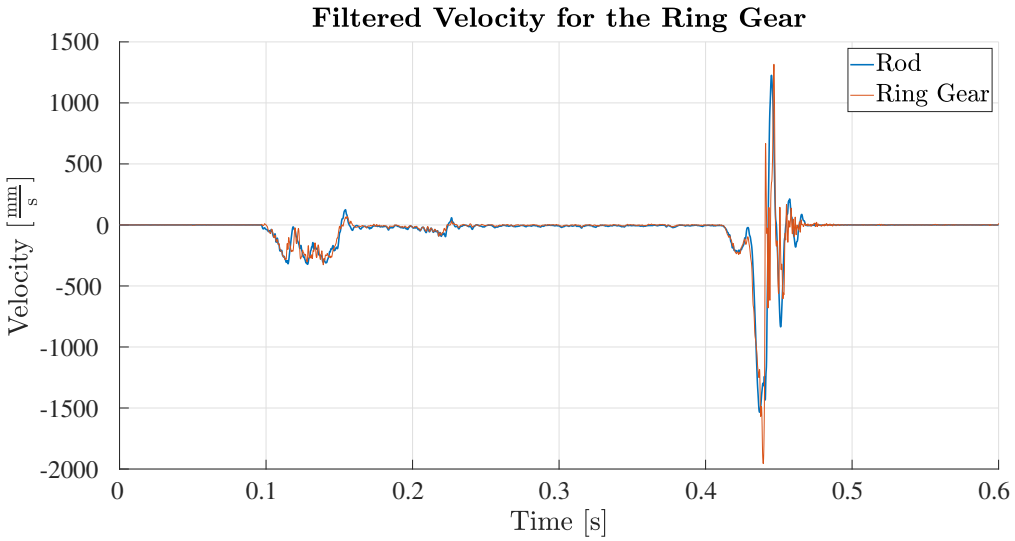


**Figure 4.8:** The velocity of the rod and ring gear for the entire shift process for case 53. The velocities have been filtered.

In summary, the velocities of the rod and ring gear demonstrate a correlation throughout the entirety of the gear change process. However, notable differences exist between the two components and the three cases. The ring gear exhibits greater fluctuation and experiences more rapid changes in velocity, both in terms of increases and decreases, compared to the rod. Consequently, the ring gear displays a more pronounced back-and-forth motion during the shift, whereas the motion of

the rod appears to be steadier and more consistent. The absolute velocities of the components tend to differ between the cases.

## 4.2 Initial conditions

When determining the initial conditions needed to replicate the provided empirical test data, different approaches were investigated. The different methods are discussed further in Chapter 5. The synchronisation gives a relative motion between the ring gear and rod that is not included in the FE model. The results of using 1 weighted velocity and 3 velocities are shown below.

### 4.2.1 Single velocity

When investigating how the weighted velocity stands compared to the velocity of the rod and ring gear respectively, the results are shown in Figure 4.9. The scatter plot displays that the weighted velocity has a linear correlation between the rod and ring gear velocity. The blue dots are the rod velocity, the red dots are the ring gear velocity and the black dots are the weighted velocity. The velocities are plotted against the first rebound distance calculated from the empirical test data of the wall hit in the final stage of the shift process. The weighted velocity has a linear behaviour and it is gathered in the middle of the rod and ring gear velocities.

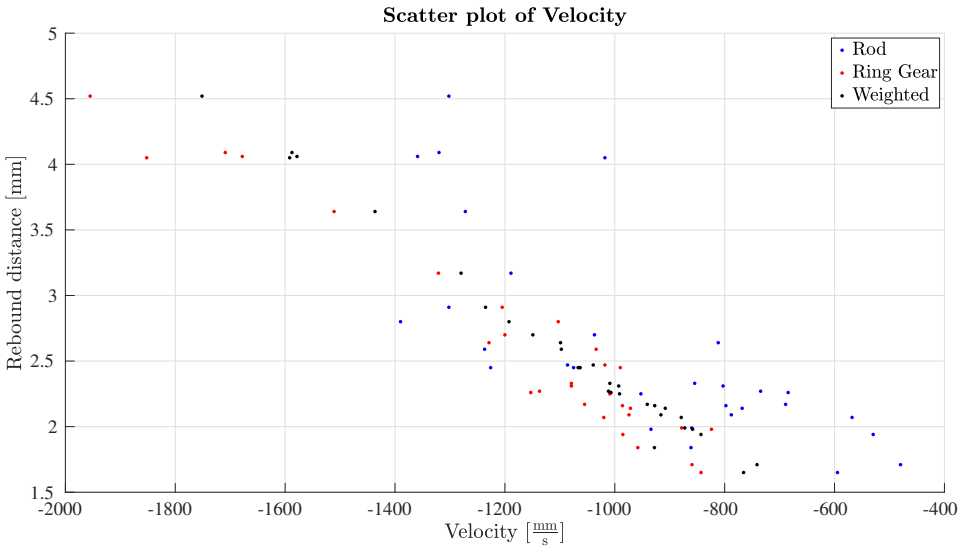


**Figure 4.9:** Scatter plot of the rod, ring gear and weighted velocity respectively.

When comparing the weighted average velocity against the average value of the velocities of the rod and ring gear, the results are shown in Figure 4.10. The weighted velocity most often has a larger absolute value.

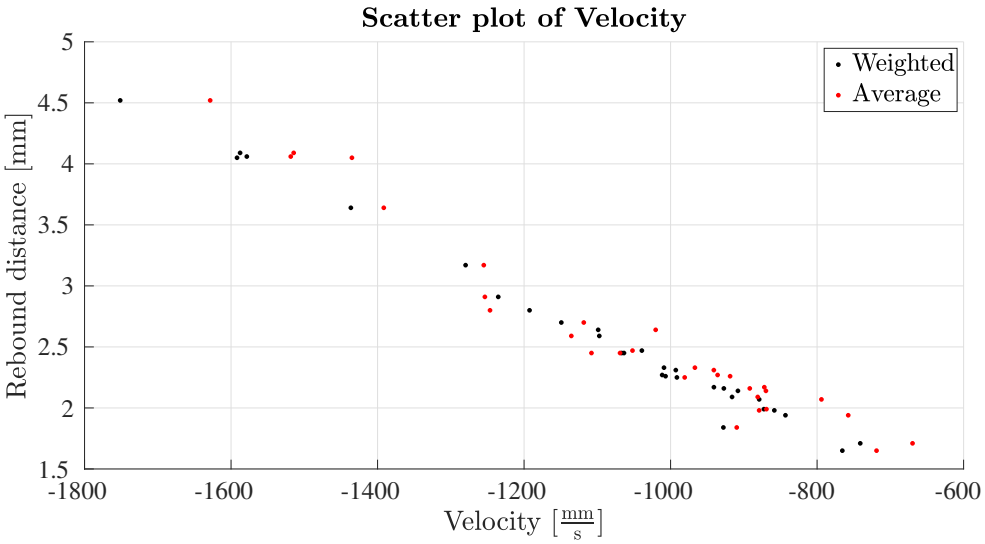


**Figure 4.10:** A comparison of the weighted average velocity vs the average velocity.

The observed correlation suggests that the velocity thereby improves the accuracy of the velocity distribution in the model with regard to the mass of the system. The ring gear possesses a higher mass and, in the majority of the gear shifts, a higher absolute velocity

### 4.2.2 Multiple velocities

When assessing whether the model aligns more closely with 3 independent initial velocities as opposed to 1 weighted velocity, a study was conducted. Using 3 independent velocities would introduce inconsistent starting conditions in the model that will introduce oscillations between the rod and ring gear. The components would move at different velocities. The bar diagram compares the displacement of the first oscillation from the performed simulations with the displacement from the empirical test data for each case. Hence, the $y$-axis contains the error from the simulations. The blue bars are the simulations with 1 weighted average velocity, and the orange bars are the results from the simulations using 3 velocities. As Figure 4.11 shows, the simulations using 1 velocity align better with the empirical test data for 8 out of the 10 tested cases. However, this study only contains 10 cases. It indicates that using 1 velocity yields more closely corresponding results, but to be sure a larger study should be conducted

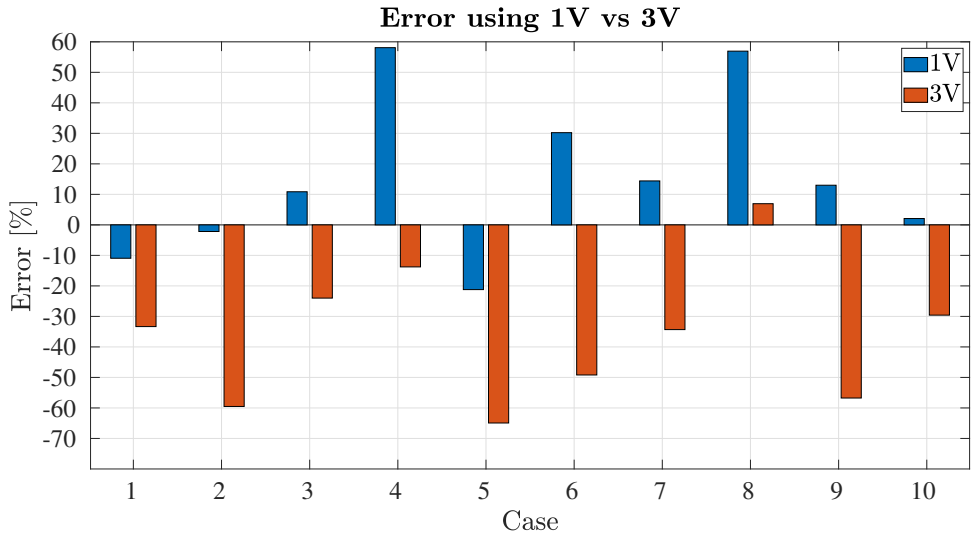


**Figure 4.11:** A bar chart comparing the results of the displacement of the first oscillation for the simulations using either 1 or 3 velocities. The zero level is the displacement from the test data.

## 4.3 Damping

The model required energy dissipation to closely match the empirical test data. Therefore, contact damping was implemented for the material involved in the impact. An iterative approach was adopted, analysing damping coefficient values of 0.01 $\frac{\text{Ns}}{\text{mm}}$, 0.05 $\frac{\text{Ns}}{\text{mm}}$, 0.1 $\frac{\text{Ns}}{\text{mm}}$, and 0.5 $\frac{\text{Ns}}{\text{mm}}$. An extract of the findings of this analysis is summarised in Table 4.2. The table, in full, is found in Appendix A.1.

The table presents the displacement values of the first two peaks in the oscillations, along with their corresponding error values. These peak values represent the magnitude of the oscillations observed in the system.

| **Case** | **CD** [$\frac{\text{Ns}}{\text{mm}}$] | **Peak 1** [mm] | **Peak 2** [mm] | **Error 1** [%] | **Error 2** [%] |
|---|---|---|---|---|---|
| 1 | 0.01 | 2.09 | 1.76 | 7 | 4 |
| 1 | 0.05 | 2.07 | 1.71 | 8 | 0.5 |
| 1 | 0.1 | 2.05 | 1.72 | 9 | 1 |
| 1 | 0.5 | 1.86 | 1.35 | 17 | 21 |
| 3 | 0.01 | 2.02 | 1.54 | 3 | 3 |
| 3 | 0.05 | 2.0 | 1.51 | 4 | 0.7 |
| 3 | 0.1 | 1.98 | 1.54 | 6 | 3 |
| 3 | 0.5 | 4.59 | 5.2 | 220 | 347 |

**Table 4.2:** An excerpt of the analysis to determine the contact damping coefficient of the system.

As indicated by the table, simulations using a contact damping coefficient of 0.5 $\frac{\text{Ns}}{\text{mm}}$

do not accurately replicate the magnitude of the oscillations observed in the test data for the selected cases. In the table, Error 1 corresponds to the error for the first peak meanwhile Error 2 refers to the error for the second peak.

The simulations employing a coefficient of 0.5 $\frac{\text{Ns}}{\text{mm}}$ possesses the highest error values. Additionally, higher damping coefficients resulted in longer simulation times. Table 4.2 highlights that simulations using a contact damping coefficient of 0.05 $\frac{\text{Ns}}{\text{mm}}$ demonstrate the closest alignment with the corresponding test data.

## 4.4 Simulation results

When analysing the results from the simulations, data has been compared between the simulation results and the empirical test data to tune and validate the FE model. In this section, all of the results are presented and analysed. The simulations have yielded results for the displacement of the rod and ring gear, as well as the strain experienced by the fork.

### 4.4.1 Displacement

After performing the simulations, a behaviour where the oscillations are disrupted was detected. This was, for example, observed in case 30. Figure 4.12 displays this behaviour. The figure shows the comparison between the test data for the rod position and the simulated position for the rod. After conducting the simulation for all of the 30 different cases, the displacement of the first and second rebound distances was analysed. The results are presented in a bar chart in Figure 4.13.

The general behaviour in Figure 4.12 for the first peak and affiliated valleys corresponds well to the test data. The issue is that the progression of the simulated system is faster than the test data. The behaviour between time 0.475 s and 0.48 s where the simulated position is approximately constant also differs from what was found from the empirical data.

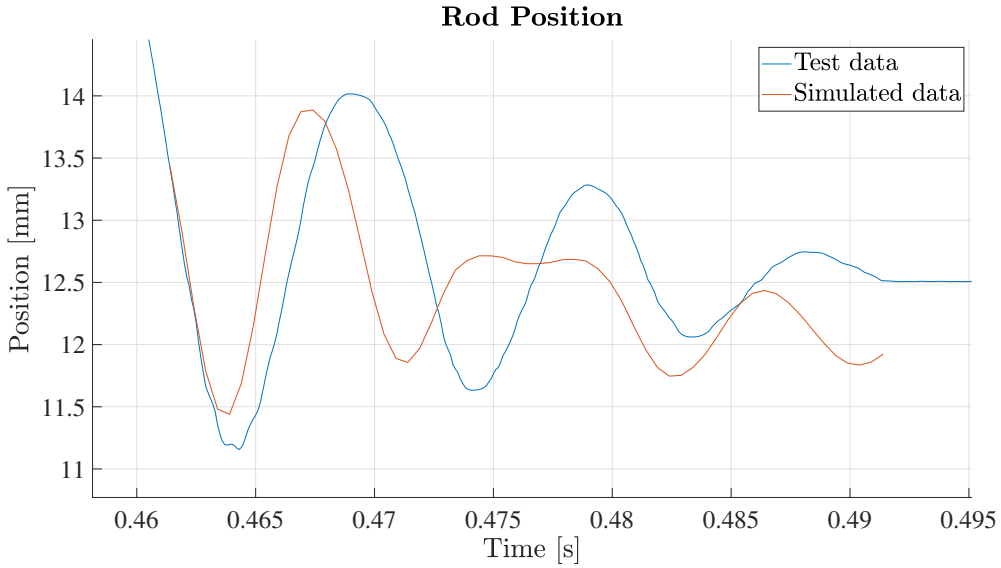


**Figure 4.12:** Rod position for test data and simulated data.

In Figure 4.13, the $y$-axis consists of the percentage error concerning the corresponding rebound distance observed in the empirical test data for each shift. The average error for the first rebound distance is 20 %. For the second oscillation, the average error is 32 %.

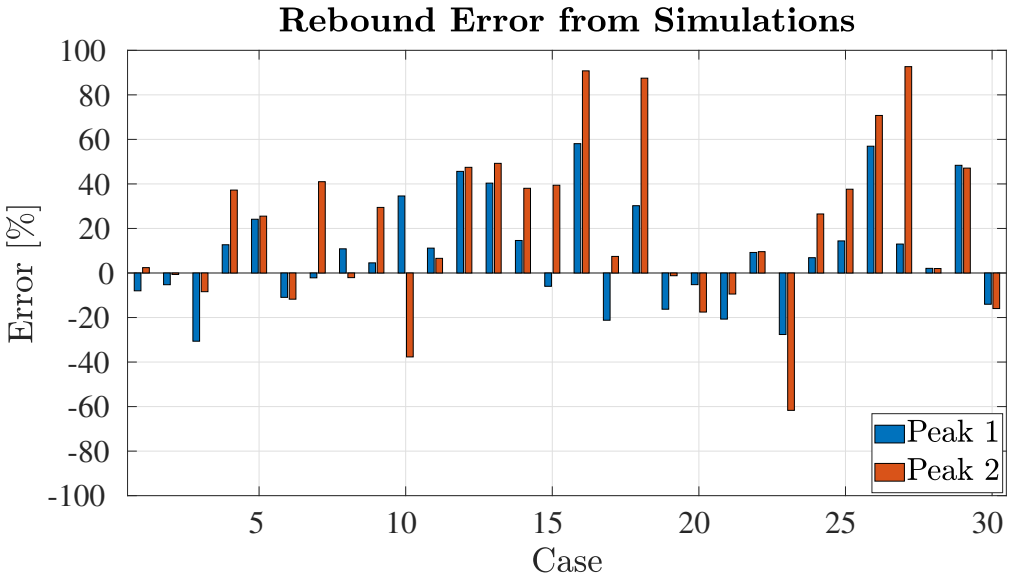


**Figure 4.13:** A bar chart presenting the results of the rebound error for the first 2 oscillations from the simulations. The zero level is the test data.

Figure 4.13 reveals a broad range of results, with errors spanning from nearly 90 % in some cases to cases with an error percentage of approximate 1 %. In general, the first rebound distance aligns better with the test data compared to the second rebound distance. The system is set up to fit the first rebound distance since the simulations resulted in disturbances in the oscillations for some of the shifts. The

built system is unable to damp out the system in a similar way as what the real transmission does. Figure 4.14 shows this for one selected shift. The comparison is made for empirical test data and simulation for the same case.

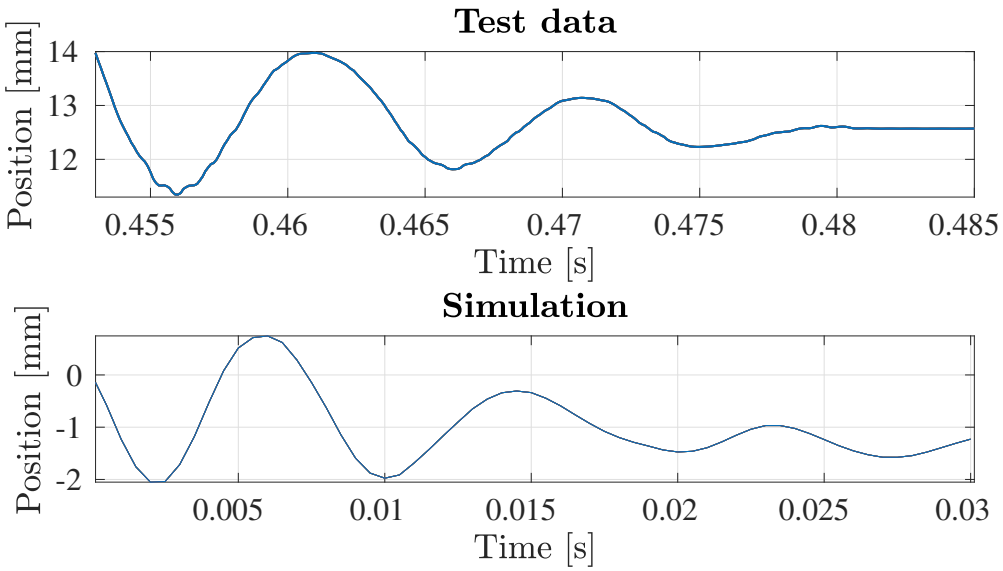


**Figure 4.14:** A subplot presenting the difference in damping for the test data and the simulations.

In alternative simulated gear exchanges, oscillations appear disrupted, as depicted in Figure 4.15. Not all simulations exhibit this behaviour, suggesting that it may originate from the spring and the natural oscillations within the system being out of sync. How the ring gear contacts and releases from the end-wall could also contribute to this behaviour.

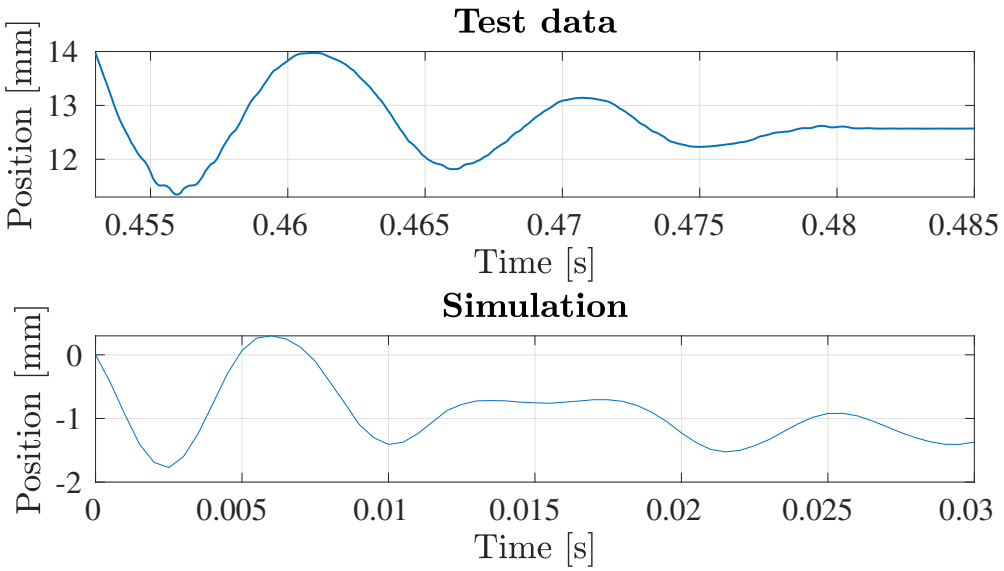


**Figure 4.15:** A subplot presenting the difference in oscillations between the test data and the simulations.

### 4.4.2 Measured and simulated strain comparison

The strain from the different simulations was extracted using the strain gauge tool in META post processor. It was measured in the same locations where the physical strain gauges were mounted during the testing. Figures 4.16-4.18 show both the empirically measured strain and the simulated results. Figure 4.16 shows the full bridge strain located at the top of the shift fork, while Figures 4.17 and 4.18 show the half bridges located on each arm of the shift fork.

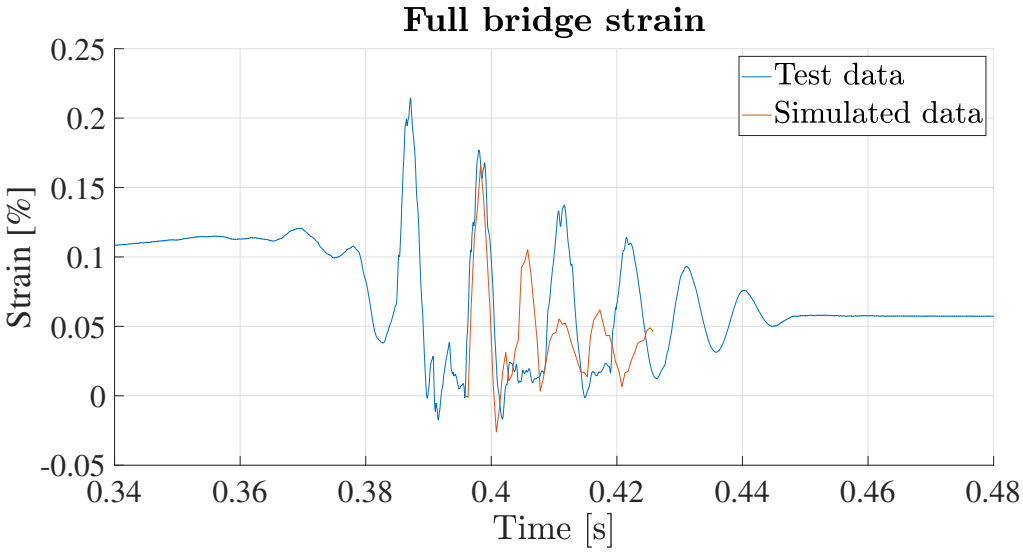


**Figure 4.16:** Test strain vs. simulated strain in the full strain bridge.

The first strain peak in the full bridge after contact corresponds well between the

empirical and simulated data, both in magnitude and duration. However, the next peak appears earlier in the simulation than in the test data.

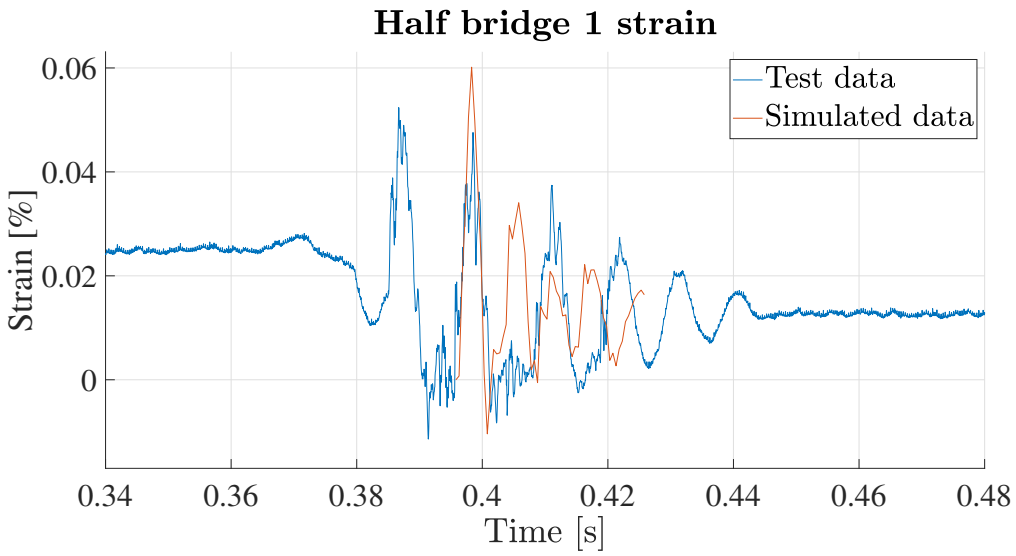


**Figure 4.17:** Test strain vs. simulated strain in the first half strain bridge.

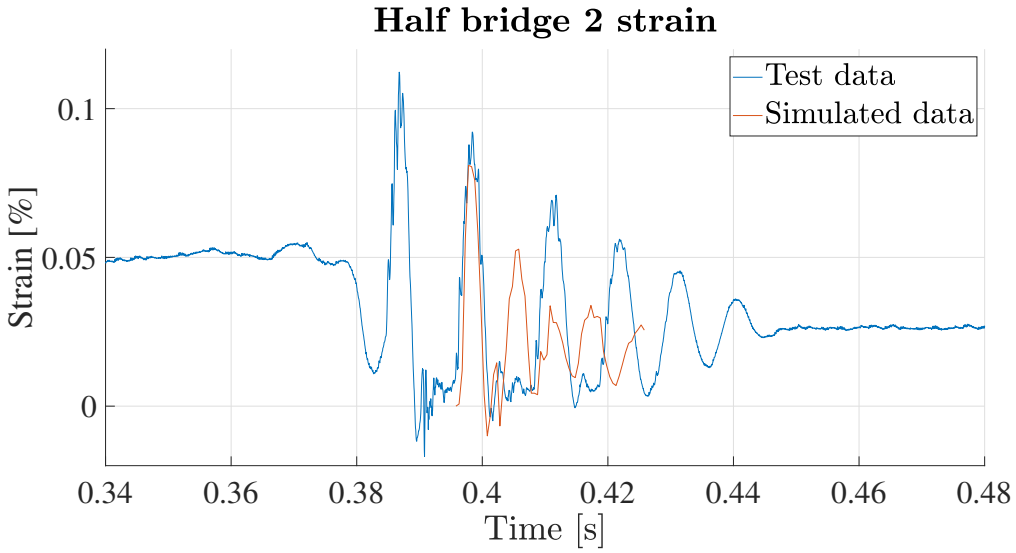


**Figure 4.18:** Test strain vs. simulated strain in the second half strain bridge.

The same behaviour as in the full bridge can be seen in the half bridge plots. The first peak corresponds well, with subsequent peaks appearing earlier. The progression is faster in the model than in the tests, which corresponds to what is seen in the rod position plot in Figure 4.12. It can also be seen that after the first peak, there is a short period where the strain is approximately 0, before increasing again, which is not captured by the model. It could partially be caused by mechanical play that affects the system each time the load changes direction.

## 4.5 Multivariate regression

A multivariate regression analysis was carried out for both the end-stop shift and the tooth collision shift. This was done using Microsoft Excels regression function by selecting an output, and several inputs in the form of data points from the test data.

### 4.5.1 Tooth collision shift

Using the variables stated in Section 3.6 with the full bridge strain as an independent variable, Excel produces a regression with a multiple R-value of 0.820 and an adjusted R-squared value of 0.535. The coefficients and P-values of the dependent variables are shown in Table 4.3 below.

| Variable Name | Coefficient | P-value |
|---|---|---|
| Ring velocity | -0.445 | 0.634 |
| Ring acceleration | -0.00105 | 0.264 |
| Rod velocity | -1.391 | 0.0133 |
| Rod acceleration | -0.000150 | 0.867 |
| Main shaft rotational velocity | -2.626 | 0.106 |
| Output shaft rotational velocity | 10.541 | 0.123 |
| Net force | 0.584 | 0.319 |
| Ring position at clash | 361.089 | 0.00129 |

**Table 4.3:** Summary of the resulting coefficient and P-value of each dependent variable in the initial multivariate regression for a shift with a tooth collision.

From the table, it is shown that the P-value of the variables Ring velocity, Rod acceleration, and Net force are large and significantly larger than the confidence level of 0.05, which means that they are statistically insignificant. Some of the other variables also have values larger than this however, only a few are removed at a time. Therefore, the mentioned variables are removed and a new regression is created.

The reason that these variables have the largest P-value is likely that they are based on each other. The ring velocity and acceleration are for example both calculated from the rod velocity, which means that only one of these is required to capture the behaviour.

The second regression has a multiple R-value of 0.801 and an adjusted R-squared value of 0.560. The resulting coefficients and P-values are summarized in Table 4.4 below.

| Variable Name | Coefficient | P-value |
|---|---|---|
| Ring acceleration | -0.00161 | 0.0298 |
| Rod velocity | 0.309 | 0.000121 |
| Main shaft rotational velocity | -2.192 | 0.139 |
| Output shaft rotational velocity | 9.831 | 0.131 |
| Ring position at clash | 353.343 | 0.000103 |

**Table 4.4:** Summary of the resulting coefficient and P-value of each dependent variable in the second multivariate regression for a shift with a tooth collision.

Now, the P-values of the output and main shaft rotational velocity are the largest and are thus removed from the regression.

The third regression after the rotational velocities have been removed gives a multiple-R value of 0.775 and an adjusted R-squared of 0.551. Table 4.5 shows the resulting coefficients and P-values of the parameters.

| Variable Name | Coefficient | P-value |
|---|---|---|
| Ring acceleration | -0.00178 | $7.518 \times 10^{-5}$ |
| Rod velocity | -1.486 | $1.505 \times 10^{-5}$ |
| Ring position at clash | 358.961 | $3.880 \times 10^{-5}$ |

**Table 4.5:** Summary of the resulting coefficient and P-value of each dependent variable in the third multivariate regression for a shift with a tooth collision.

This final regression model has decreased the multiple R-value from 0.820 to 0.775 and increased the adjusted R-squared from 0.535 to 0.551 while removing 5 parameters. The reduction in the number of parameters lets the regression be used with less data, which means that fewer measurements are required to use it. The final equation for predicting the strain in a tooth collision shift becomes:

$$\varepsilon_{Fork} = -6833.786 - 0.00178 \times a - 1.486 \times b + 358.961 \times c \tag{4.1}$$

where the first term is the intersection value, $a$ is the ring acceleration, $b$ is the rod velocity and $c$ is the Ring position at clash.

The multiple R-value of 0.775 shows that there is a somewhat strong linear relationship between the input and output variables, which verifies that a linear regression model can be used for this problem. Further, an adjusted R squared of 0.551 means that 55 % of the variation in the strain is explained by the dependent variables. This still means that some of the variation is still unaccounted for, and there is likely an additional variable that is required to better describe all of the variation. This value is lower than preferred.

### 4.5.2 End-stop shift

Similarly to the previous section, a regression model was also made for shifts that do not contain teeth clashes. Here however, since the progression without teeth clashes is less complex, fewer variables were used.

The used variables can be seen in Section 3.6.1. This gives a multiple R-value of 0.854 and an adjusted R-value of 0.699. The coefficients and P-values are presented in Table 4.6 below.

| Variable Name | Coefficient | P-value |
|---|---|---|
| Rod velocity squared | 0.000275 | 0.000325 |
| Ring velocity squared | 0.000132 | 0.00964 |
| Ring acceleration | $-4.784 \times 10^{-5}$ | 0.764 |

**Table 4.6:** Summary of the resulting coefficient and P-value of each dependent variable in the first multivariate regression for the wall hit.

The P-value of the ring acceleration is large and is therefore removed. The final resulting regression gives a multiple R-value of 0.854 and an adjusted R-squared value of 0.709.

| Variable Name | Coefficient | P-value |
|---|---|---|
| Rod velocity squared | 0.000280 | 0.000126 |
| Ring velocity squared | 0.000139 | 0.00187 |

**Table 4.7:** Summary of the resulting coefficient and P-value of each dependent variable in the second multivariate regression for the wall hit.

Table 4.7 shows that both variables have P-values significantly below 0.05. This regression result in the equation:

$$\varepsilon_{Fork} = 1039.71 + 0.000280 \times a + 0.000139 \times b \tag{4.2}$$

where 1039.71 is the intersect value, $a$ is the rod velocity squared and $b$ is the ring velocity squared.

In this regression, both the multiple R-values and adjusted R-squared values are higher than for the tooth collision shift regression. This is expected since the end-stop collision shift is less complex than the tooth collision shift, and a better fit can therefore likely be found using fewer parameters.

# 5

# Discussion

This chapter includes discussions regarding the results, approach and what needs to be further investigated. Many variables and approaches can be used in both the extraction of test data and the construction of the FE analysis. These can be altered to potentially build a model that more accurately simulates the real world scenario. Several sources of error and simplifications can explain differences between the results and the test data. Lastly, the fit of the multivariate regression model is discussed.

## 5.1 Test data

The project relies heavily on empirical test data as its foundation. Both the simulation and the multivariate regression models are constructed based on parameters extracted from the test data, making the selection of the parameters a crucial aspect of the project. Specifically, in the simulation, input values such as velocity and net force are extracted at the moment of the final collision, while in the multivariate regression, parameters are selected at the occurrence of teeth collision.

The timing of parameter extraction is therefore fundamental, yet it introduces uncertainty into the project. Fluctuations in acceleration trends and sudden changes in velocity or displacement during gear shifts can lead to unexpected oscillations, making the precise selection of timing challenging. The human error further compounds this issue, as even a small deviation of 0.001 seconds in timing can result in velocity changes of up to approximately 100 $\frac{\text{mm}}{\text{s}}$.

To enhance the accuracy of the model, it may be beneficial to explore methods to improve the precision of event timing selection. One potential approach could involve a closer analysis of acceleration graphs, which may offer more precise timing information. However, interpreting acceleration graphs can be complex due to their fluctuating nature. However, a zero value in acceleration indicates that there is no change in the velocity of the object, either because the object is stationarity or is moving with a constant velocity. By improving the accuracy of the timing of the crucial events in the gear shift, the predictive precision of the models presented here could improve.

## 5.2 Simulation

When setting up the simulation model, a lot of decisions were made. In the following section, a discussion is held about how different choices for setting up the system could have affected the results.

### 5.2.1 Mesh size

The model built has a coarse mesh. A finer mesh would most likely result in more accurate results when it comes to the strain analysis. However, a finer mesh would increase the simulation time drastically and therefore prolong the projects since a lot of simulations have had to be done. However, one simulation was done with a finer mesh in the areas where the strain gauges are placed. The simulation aimed to investigate if a finer mesh would capture the strain more similarly to the empirical test data. The duration of the simulation was 17 hours and the result yielded a significantly lower maximum strain for the full bridge strain gauge. A mesh convergence study would be interesting to perform to verify the accuracy of the FEA simulations and to enhance confidence and reliability in the performed simulations.

### 5.2.2 Boundary conditions

The ring gear is constrained by the planets in the planetary gear set which prevents any tilting of the ring gear. During the ANSA model setup, two distinct methods were considered for applying the boundary condition to emulate the constraint between the ring gear and the planetary gear set. These methods involved either utilizing a kinematic coupling or introducing an extruded cylinder. The way of creating the imitated cylinder was the same as when the housings were created, see Section 3.2.4.

Using an extruded cylinder, the extruded surface, and not the ring gear inner surface, is allowed to translate in the $z$-direction due to applied boundary conditions. A contact pair is subsequently implemented between the surface from which the extruded cylinder was generated, and the extruded surface. This contact pair was frictionless.

The other option was to create a kinematic coupling on the inside surface of the ring gear. The coupling is then connected to a node placed in the centre of the ring gear. The slave nodes were free to move in the $z$-translation direction. Furthermore, a boundary condition was applied on the reference node locking the coupling in DOFs 12456.

The method used in the project is the kinematic coupling approach due to the ease of implementation. The advantages of using a kinematic coupling instead of an extruded cylinder are mainly the manageability as well as kinematic method doesn't require more elements in the model. More elements can prolong the solver time for the simulation since the added elements can be smaller than the current smallest element. Furthermore, the added elements for the extruded cylinder can

result in problems with the chosen mesh properties. Another advantage is that the kinematic coupling method doesn't require more contact pairs. The extruded cylinder approach would need an additional contact pair between the surface of the extruded surface and the ring gear.

### 5.2.3 Damping

One challenge encountered in the simulation is related to the damping. The system is in deficit of damping, relying only on a combination of Rayleigh- and contact damping. Due to time constraints, the determination of the contact damping coefficient was expedited, resulting in a less accurate representation of the damping in the system. A more detailed analysis would have provided a better understanding of the system's damping characteristics and therefore improved the results of the simulations. The values tested in the performed analysis showed that higher coefficient values resulted in longer simulation time, with variations up to 515% observed for the same case with different coefficients. A higher value of the contact damping coefficient generally decreases the oscillations, except for the coefficient of 0.5, which unexpectedly increases the oscillations. The coefficient seems to result in numerical errors. The contact damping coefficient therefore does not behave as expected and would require a deeper analysis.

Another part affecting the damping is the spring element which emulates the variable force on the rod. The spring may cause the oscillations to propagate instead of reduce as the ring makes contact with the wall. To resolve this issue, an additional damping element could be used to counteract the spring. It may also be possible to model the variable force in another way that does not contribute to the oscillations. Figure 4.12 shows that the behaviour of the position of the rod is not fully captured by the model. This is also something that could be affected by the spring. The spring may prevent the natural oscillation of the position after the impact, causing the position to become approximately constant over two cycles, as seen in Figure 4.12. This could however also be the result of the ring gear moving in the opposite direction of the rod, preventing the expected motion.

Another way of improving the system's damping could be to explore the influence that the house may have on the damping. The housings likely absorb energy which in turn damps the system, this could be a distinction from the real life scenario. Another part of the system that isn't taken into consideration is the thermal damping from the pneumatic cylinder, this is however unlikely to affect the results in a significant matter. To analyse the housings, a static simulation containing the spring and the contact damping coefficient could have yielded valuable insights and helped improve the dynamic explicit simulation by analysing the energy of the system and how it disperses.

### 5.2.4 Velocities

When implementing the initial conditions in ANSA, a discussion was held about whether the most representable method would be to use 1 or 3 velocities for the different moving PIDs. The velocity of the rod was given from the empirical test data and the velocity of the ring gear was calculated, see Section 3.3.2.

The usage of multiple initial velocities represents the real life scenario more accurately. However, the initial velocity on the fork would still need to be weighted depending on the mass of the system between the 2 known velocities, rod and ring gear. The other choice was to use one initial velocity for all of the moving parts in the simulation by taking a weighted average, based on the mass of the parts and their velocities.

The reason that the different parts have different velocities is that when the synchronisation occurs, the load is still applied to the rod while the ring gear is held in place. This causes the fork to bend. When the ring gear is released from the synchronisation, the bent fork springs back, giving different initial velocities. This is not fully captured by using 1 or 3 initial velocities. One way it could have been performed is to first have a static simulation step that includes the flexing of the fork, to then be let go into the dynamic step.

The disadvantage of using multiple initial velocities is that it would be more difficult to calibrate to imitate the test data since more input parameters introduce complexity. There is also uncertainty in how the parts move relative to each other which could lead to the the different parts moving out of synchronization and impacting the displacement of the system in an unwanted way.

#### 5.2.4.1 The impact of acceleration

An investigation was made if there was a clear connection between the acceleration, weighted velocity, and the first rebound distance of the test data. A 3-dimensional plot in MATLAB was created based on the given empirical test data. The results are shown in Figure 5.1. The velocities are mostly gathered in the range of $-800\,\frac{\text{mm}}{\text{s}}$ to $-1200\,\frac{\text{mm}}{\text{s}}$ and the acceleration differs from $200\,000\,\frac{\text{mm}}{\text{s}^2}$ to $-200\,000\,\frac{\text{mm}}{\text{s}^2}$. The rebound distance is larger for the cases with a higher absolute velocity. Higher accelerations might be expected to result in greater rebound distance due to the increased forces exerted on the system. However, in the context of the provided data, this expected correlation was not observed.

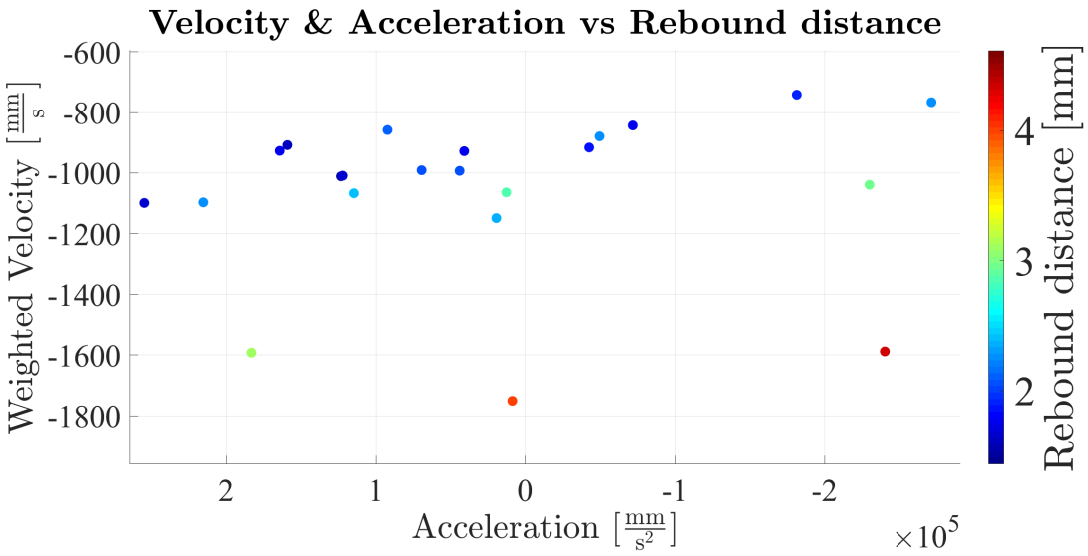


**Figure 5.1:** A 3-dimensional plot of the acceleration, velocity, and rebound distance of the rod for the empirical test data. The third dimension is shown with a colour bar in correlation with the colours of the figure markers to show the rebound distance.

This lack of observed connection between acceleration and rebound distance suggests that other factors may be more influential in determining the rebound distance of the rod in the system. Other factors may play a more dominant role than the acceleration alone. However, the velocity impacts the rebound distance heavily.

### 5.2.5 Fluctuations

One aspect that has been discussed during the project is the movement of the ring gears position and rotation during the shift. The occurrence of fluctuations in the ring gear and the origin of these alternations has resulted in an analysis trying to determine the difference in displacement of the arms of the fork. As mentioned in Section 4.1.1, one of the reasons for the fluctuations is most likely the unsymmetrical geometry of the fork which leads to a difference in stiffness in the fork arms. The fork then starts to oscillate resulting in the fluctuations seen in Figure 4.4. However, it was determined that the effects of these fluctuations were too insignificant for the project to justify the time needed to proceed with this analysis. This analysis would however be interesting for future work.

## 5.3 Regression

From the two separate regressions, it is found that the adjusted R squared is lower than preferred. For the tooth collision shift and end-stop collision shift, 45 % and 29 % respectively of the variance in the strain is not explained by the dependent variables. This may be the result of that certain variables would be required to explain the strain that is not present in the regression. It could also be caused by using incorrect dependent variables.

It has been assumed that the relationship between the dependent and independent variables is linear. This may not be completely accurate. Despite reaching large multiple R values, there could be some non-linearities between some of the variables and the strain that is unaccounted for, which would also reduce the quality of the regression. This may especially be true for the tooth collision shift, since both the multiple R and adjusted R squared are lower than for a shift with an end-stop collision.

## 5.4 Error sources

Throughout the project, several uncertainties have arisen. Modifications have been made to the given geometry for simplification. These changes have however affected the results. Moreover, the project's tentative nature is imminent due to the complexity of the given empirical data. Although external factors such as oil temperature and that there is the same gear change, high to low gear, throughout the project are the same, each dataset possesses its unique characteristics. Every shift is therefore unique.

### 5.4.1 Uniqueness of every shift

The unique characteristics that each shift provides give uncertainty to the project. At the beginning of each shift, the ring gear is subjected to a rotational synchronisation before proceeding with the shifting process. This synchronisation varies in duration resulting in different time schedules for each shift. Consequently, this variance affects the consistency across shifts. During the shift process, the ring gear can come in contact with other components disrupting the movement of the system, potentially causing axial motions to transition into rotational motion. Such rotations have significant ramifications on data parameters crucial for the project, including velocity, acceleration, and displacement. Furthermore, the unpredictability of each shift is the occurrence of teeth hit. The number of hits and location of these impacts directly influence the velocity of the system which is one of the main parameters used in the project to predict strain. During each contact between the teeth, friction occurs which contributes to damping in the system in terms of energy loss with regards to heat. All of this results in unforeseeable consequences and makes every shift unique.

### 5.4.2 General error sources

The main error sources in the project are concerning how the data either is read or calculated. A lot of variables depend on each other, for example, the displacement of the ring is dependent on the fork displacement which in turn is calculated from the given strain data and rod displacement. Hence, some data is determined based on one another, and if the first extracted data point is at all erroneous, data derived from it is also incorrect. Another important aspect is the time instant used for when the data is extracted. Small changes in the time instant can lead to significant

changes in the data used for the simulation and the regression. The time instants play a vital role in the project while it is a big uncertainty. It would be optimal to define a set of parameters from the shift that could be used in a script to ensure that the data is taken from the same point in each shift, regardless of in which time instant it occurs. This would potentially remove one factor of uncertainty from the project and the models created.

# 6
# Conclusion

This project aimed to create a dynamic FE model of a shift in the range section of a truck's transmission. It further aimed to investigate which parameters are key to predicting the behaviour of the shift fork during a shift.

It has been found that the most important parameter in the shifting sequence is the axial velocity when the ring gear impacts the housing. This is mainly what determines the rebound distance the rod, fork and ring gear are subjected to, and how much strain in the fork it causes. Thus, the velocity has been used as an input parameter in the FE model to more closely resemble the real system. Another input parameter to the FE model is the net force remaining in the system after the spring has been considered. However, this force doesn't vary much in comparison to the variation in velocity and is not affecting the results equally.

The created FE model correlates to the empirical data regarding the first displacement peak well. Also, the strain results here are similar. After this initial peak, the result diverges from the test data. To improve the model, a further investigation of the damping of the system needs to be conducted. An error in the damping is likely what causes the model results and the test data to correlate less well as the simulation progresses. Despite this, an explicit dynamic model of the shift fork seems to be viable to get accurate results that correspond to the test data.

Through analysis, parameters like acceleration and rotational velocity are less influential to the rebound distance and strain for both shift types with tooth and end-stop collision. However, this may partially depend on uncertainties when extracting test data.

The resulting multivariate regressions created yielded a somewhat reliable strain prediction, however, given the low adjusted R squared value, the model would need to be refined to have more certainty in the predictions. Especially for the tooth collision shift, where more factors are of importance than in the end-stop collision shift. There is likely some variable or variables that should be included for a better fit, that currently are not included. It is also possible that the extracted data used needs to be revised for a more robust regression.

In summary, this project has resulted in a foundation of models that could be used to predict strain in the shift fork, and an analysis of what parameters are of importance. These models can further be developed and improved to achieve a closer resemblance

to the measured test data.

# Bibliography


[1] Pawel M Kurowski. *Finite Element Analysis for Design Engineers: Vol. Second edition.* SAE International, 2017.

[2] F. Colin C. *Using Finite Element Analysis Throughout The Product Development Cycle for Plastic Interior Trim Components*. SAE Technical Paper 950640, 1995. URL: https://doi-org.proxy.lib.chalmers.se/10.4271/950640.

[3] Alexander Pett. "What is Explicit Dynamics?" In: *Ansys Inc* (Mar. 2024). URL: https://www.ansys.com/blog/what-is-explicit-dynamics.

[4] Ajay Harish. "Implicit vs. Explicit FEM: What Is the Difference? | SimScale". In: *SimScale* (Mar. 2024). URL: https://www.simscale.com/blog/implicit-vs-explicit-fem.

[5] *ABAQUS Analysis User's Manual (v6.6)*. [Online; accessed 27. Mar. 2024]. Mar. 2024. URL: https://classes.engineering.wustl.edu/2009/spring/mase5513/abaqus/docs/v6.6/books/usb/default.htm?startat=pt09ch29s02aus118.html.

[6] *SIMULIA Online User Assistance - Contact damping*. [Online; accessed 27. Mar. 2024]. Feb. 2020. URL: https://cae.it.volvo.net/v2021/English/DSSIMULIA_Established.htm?show=SIMACAEITNRefMap/simaitn-c-contactdamping.htm.

[7] *ABAQUS Analysis User's Manual (v6.6)*. [Online; accessed 27. Mar. 2024]. Mar. 2024. URL: https://classes.engineering.wustl.edu/2009/spring/mase5513/abaqus/docs/v6.6/books/usb/default.htm?startat=pt09ch30s01aus140.html.

[8] *Computing Rayleigh Damping Coefficients | Knowledge Base | SimScale*. [Online; accessed 27. Mar. 2024]. Feb. 2022. URL: https://www.simscale.com/knowledge-base/rayleigh-damping-coefficients.

[9] *Structural_Dynamics_with_Linear_System_Theories_16nov20.pdf: TME141 Structural dynamics*. [Online; accessed 27. Mar. 2024]. Mar. 2024. URL: https://chalmers.instructure.com/courses/21162/files/2390214?module_item_id=319142.

[10] *ABAQUS Analysis User's Manual (v6.5-1)*. [Online; accessed 27. Mar. 2024]. Mar. 2024. URL: https://classes.engineering.wustl.edu/2009/spring/mase5513/abaqus/docs/v6.5/books/usb/default.htm.

[11] *Getting Started with ABAQUS/Explicit: Keywords Version (v6.5-1)*. [Online; accessed 27. Mar. 2024]. Mar. 2024. URL: https://classes.engineering.wustl.edu/2009/spring/mase5513/abaqus/docs/v6.5/books/gsx/default.htm?startat=ch03s03.html.

[12] *ABAQUS/CAE User's Manual (v6.6)*. [Online; accessed 27. Mar. 2024]. Mar. 2024. URL: https://classes.engineering.wustl.edu/2009/spring/mase5513/abaqus/docs/v6.6/books/usi/default.htm?startat=pt03ch17s06s01.html.

[13] *Abaqus*. [Online; accessed 27. Mar. 2024]. Mar. 2024. URL: https://2021.help.altair.com/2021/hwdesktop/cfd/topics/pre_processing/meshing/element_quality_calculations_abaqus_r.htm.

[14] Bill Webster. "Hourglassing and Shear Locking - What Are They And Why Does It Matter?" In: *Fidelis* (Mar. 2021). URL: https://www.fidelisfea.com/post/hourglassing-and-shear-locking-what-is-it-and-why-does-it-matter.

[15] *Solid (continuum) elements*. [Online; accessed 27. Mar. 2024]. Mar. 2020. URL: https://cae.it.volvo.net/v2021/English/SIMACAEELMRefMap/simaelm-c-solidcont.htm.

[16] *Getting Started with ABAQUS/Standard: Keywords Version (v6.6)*. [Online; accessed 27. Mar. 2024]. Mar. 2024. URL: https://classes.engineering.wustl.edu/2009/spring/mase5513/abaqus/docs/v6.6/books/gss/default.htm?startat=ch04s01.html.

[17] Dewesoft. *Signal filtering, Signal suppression, Signal processing | Dewesoft*. [Online; accessed 27. Mar. 2024]. Mar. 2024. URL: https://training.dewesoft.com/online/course/filters.

[18] Evangelos C Alexopoulos. "Introduction to multivariate regression analysis". In: *Hippokratia* 14.Suppl 1 (2010), p. 23.

[19] Neil H. Timm. *Applied multivariate analysis*. Springer, 2011.

[20] Jim Frost. "How to Interpret P-values and Coefficients in Regression Analysis". In: *Statistics By Jim* (Mar. 2023). URL: https://statisticsbyjim.com/regression/interpret-coefficients-p-values-regression.

# A

# Appendix

## A.1 Contact damping analysis

| **Case** | **CD** [$\frac{\text{Ns}}{\text{mm}}$] | **Peak 1** [mm] | **Peak 2** [mm] | **Error 1** [%] | **Error 2** [%] |
|---|---|---|---|---|---|
| 1 | 0.01 | 2.09 | 1.76 | 7 | 4 |
| 1 | 0.05 | 2.07 | 1.71 | 8 | 0.5 |
| 1 | 0.1 | 2.05 | 1.72 | 9 | 1 |
| 1 | 0.5 | 1.86 | 1.35 | 17 | 21 |
| 3 | 0.01 | 2.02 | 1.54 | 3 | 3 |
| 3 | 0.05 | 2.0 | 1.51 | 4 | 0.7 |
| 3 | 0.1 | 1.98 | 1.54 | 6 | 3 |
| 3 | 0.5 | 4.59 | 5.2 | 220 | 347 |
| 5 | 0.01 | 3.21 | 3.76 | 42 | 7 |
| 5 | 0.05 | 3.18 | 3.71 | 44 | 8 |
| 5 | 0.1 | 3.15 | 3.59 | 45 | 11 |
| 5 | 0.5 | 3.27 | 3.92 | 40 | 3 |
| 7 | 0.01 | 2.33 | 2.04 | 14 | 41 |
| 7 | 0.05 | 2.31 | 1.99 | 13 | 37 |
| 7 | 0.1 | 2.30 | 2.01 | 12 | 38 |
| 7 | 0.5 | 6.56 | 6.17 | 320 | 425 |
| 9 | 0.01 | 2.18 | 1.73 | 25 | 23 |
| 9 | 0.05 | 2.16 | 1.71 | 24 | 21 |
| 9 | 0.1 | 2.14 | 1.78 | 23 | 26 |
| 9 | 0.5 | 2.87 | 3.44 | 65 | 144 |

**Table A.1:** Full table of the contact damping coefficient analysis.

**INSTITUTIONEN FÖR MEKANIK OCH MARITIMA VETENSKAPER**
**CHALMERS TEKNISKA HÖGSKOLA**
Göteborg, Sverige 2024
www.chalmers.se


CHALMERS
UNIVERSITY OF TECHNOLOGY